Nuclear Magnetic Resonance and Magnetic Ordering in NiF_2

R. G. SHULMAN
Bell Telephone Laboratories, Murray Hill, New Jersey, and Fysisk-Kemisk Institut, University of Copenhagen, Copenhagen, Denmark

(Received August 30, 1960)

Measurements of the nuclear magnetic resonance of the F^{19} nucleus in single crystals of NiF_2 have been made at temperatures between 4.2°K and 298°K. In the paramagnetic state at 298°K, for arbitrary directions of H_0 two resonances were observed, while for H_0 in a (100) plane only one resonance was observed as expected from the crystal symmetry. The shift of the resonances from the normal resonance field ω/γ_N allows one to calculate three independent parameters of the hyperfine interaction between the F^{19} nuclei and the magnetic electrons. In conjunction with measurements made in the antiferromagnetic state, it was possible to determine the individual components of the hyperfine interaction in units of 10^{-4} cm^{-1} as $A_s^{\rm I}=36.4\pm1.8$, $A_s^{\rm II}=42.1\pm2.1$, $A_\sigma^{\rm I}=9.1\pm0.9$, and $A_\sigma^{\rm II}=9.9\pm0.9$. Superscripts refer to the two different bonds with Ni^{++} and subscripts s and σ refer to isotropic and anisotropic contributions. From these we calculate that the fractions of unpaired spin in the corresponding fluoride ion s and p_σ orbitals are $f_s^{\rm I}=(0.46\pm0.02)\%$, $f_s^{\rm II}=(0.54\pm0.03)\%$, $f_\sigma^{\rm I}=(4.1\pm0.4)\%$, and $f_\sigma^{\rm II}=(4.5\pm0.4)\%$. Since geometrical considerations almost completely forbid magnetic p_π interactions in NiF_2, there is a negligible cancellation of p_σ interactions by the p_π so that, unlike the case for MnF_2 and FeF_2, the admixture of magnetic electrons into fluoride ion orbitals is almost completely determined.

At temperatures just above the antiferromagnetic transition $T_N=73.2$°K, the resonance shifts with H_0 in the (001) plane change rapidly with temperature. Between 75.7°K and T_N the susceptibility of one sublattice becomes negative while the other remains positive. This has been correlated with the sublattice susceptibility derived by Moriya from the spin Hamiltonian $\mathcal{H}=g\beta H+DS_z^2+E(S_x^2-S_y^2)$. By fitting the theoretical susceptibility we have determined the sign of E in this Hamiltonian.

Below 73.2° the nuclear resonances are consistent with Moriya's model in which the spins are antiparallel along [100] and tipped ~1.3° towards [010]. Ericson's description of the magnetic ordering is shown to be incorrect. In the antiferromagnetic state the F^{19} resonance broadens as H_0 is lowered below 5000 gauss.

INTRODUCTION

PREVIOUS[1,2] nuclear magnetic resonance studies of the fluorine nuclei in iron group fluorides have revealed the existence of strong hyperfine interactions between the fluorine nuclei and the magnetic electrons. These resonance experiments have been interpreted so as to provide information about the distribution of magnetic electrons in fluoride orbitals and these interpretations have yielded particularly detailed information when the magnetic ion has been Mn^{++} in the two crystals MnF_2 and[3] $KMnF_3$. It was clear that similar experiments on NiF_2 would contribute to our knowledge of the electron-nuclear interactions but these experiments had to await single crystals of NiF_2. Recently Guggenheim[4] has succeeded in growing large single crystals and has kindly placed them at our disposal. In addition to exhibiting the anisotropic nature of the hyperfine interactions, the single crystals have also made it possible to study the anisotropy of the magnetic properties. Since NiF_2 is antiferromagnetic[5] below 73.2°K and has a small ferromagnetic[6] component, the magnetic properties are really quite anisotropic.

Our results can be described in the following general fashion. In the paramagnetic region, well above the transition temperature, the nuclear resonances observed are similar to those obtained in other[1–3] paramagnetic fluorides. In this region the resonances were shifted from the normal field value of ω/γ_N by several percent to lower fields. From these shifts we have obtained quantitative values of the hyperfine interactions using the analysis previously[1,2] presented. These parameters are discussed in terms of the same parameters of the ionic bond measured in other crystals, particularly MnF_2, FeF_2, and $KMnF_3$.

As the temperature is lowered to within a few degrees of the antiferromagnetic transition very unusual effects are observed and are described below.

Finally, the F^{19} resonance is observed in the antiferromagnetic region and the antiferromagnetic ordering is determined to be quite different from the previously published results of neutron diffraction[7] studies. The ordering is shown to consist of spins aligned in the (001) plane almost exactly along the [100] or [010] directions in accordance with the analysis of magnetic ordering in NiF_2 by Moriya.[8] During the course of our experimental study of NiF_2, a theoretical investigation of the magnetic properties has been made by Moriya.[8] At the same time that our nuclear resonance studies were indicating that the magnetic ordering could not be as previously described, Moriya showed by considering the consequences of the spin Hamiltonian for NiF_2 in light of the susceptibility measurements already available[6,9] that [100] rather than [001] would be the direction of antiferromagnetic alignment. This has explained our measurements and has been confirmed by them.

CRYSTAL PREPARATION AND STRUCTURES

As mentioned above, the single crystal of NiF_2 was prepared by Guggenheim. Previously, small crystals had

[1] R. G. Shulman and V. Jaccarino, Phys. Rev. **108**, 1218 (1957).
[2] J. W. Stout and R. G. Shulman, Phys. Rev. **118**, 1136 (1960).
[3] R. G. Shulman and K. Knox, Phys. Rev. **119**, 94 (1960).
[4] H. Guggenheim, J. Phys. Chem. **64**, 938 (1960).
[5] E. Catalano and J. W. Stout, J. Chem. Phys. **23**, 1284 (1955).
[6] L. M. Matarrese and J. W. Stout, Phys. Rev. **94**, 1792 (1954).
[7] R. A. Ericson, Phys. Rev. **90**, 779 (1953).
[8] T. Moriya, Phys. Rev. **117**, 635 (1960).
[9] W. J. de Haas, B. H. Schultz, and J. Koolhaas, Physica **7**, 57 (1940).

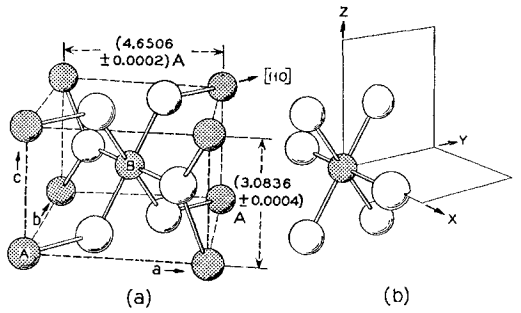

FIG. 1. Schematic diagram of unit cell of NiF_2. Black circles are Ni^{++} ions and white circles F^- ions. The origin of the crystal coordinate system (a,b,c) is chosen at the lower left corner, at Ni^{++} ion on site A. The positive x direction of the right-handed coordinate system (x,y,z) based on the Ni^{++} ions shown in Fig. 1(b) is indicated for A and B sites by a plus sign, while the positive z direction always coincides with the positive c axis. The [110] direction in our convention coincides with the positive x direction on the A site. The $[1\bar{1}0]$ has been chosen along the negative x axis of the B site. The [001] coincides with both z and c. Dimensions are taken from references 11 and 12. The two Ni^{++} ion sites A and B differ from each other only by a 90° rotation about the z axis.

been obtained by Matarrese and Stout[6] who used them to measure the magnetic anisotropy. Stout[10] had pointed out that the difficulty in growing large single crystals of NiF_2 from the melt undoubtedly arose from the high vapor pressure of NiF_2 at its melting point. The vapor pressure was probably greater than one atmosphere and a closed system was, in his opinion, desirable. Guggenheim[4] achieved this condition with a platinum crucible 8 in. long, 1-in. diameter, tapered to a point over 1 in. The walls were 0.030-in. thick platinum and the entire assembly, once loaded with NiF_2, was closed by welding the platinum.

NiF_2 is isomorphic with MnF_2, FeF_2, CoF_2, and ZnF_2. These crystals have the rutile structure which is tetragonal belonging to space group $D_{4h}^{14}-P4/mnm$ as shown in Fig. 1(a). The crystal structure has been determined by the x-ray studies of Stout and Reed[11] and more recently refined by Baur.[12] As can be seen from Fig. 1(a) the metal ions at (0,0,0) and $(\frac{1}{2},\frac{1}{2},\frac{1}{2})$ are each surrounded by six fluoride ion neighbors at $\pm(u,u,0)$ and $\pm(\frac{1}{2}+u, \frac{1}{2}-u, \frac{1}{2})$. Unit cell dimensions are given in Fig. 1(a) while the value of $u=0.304\pm0.002$ has been given by Stout.[2] Each Ni^{++} ion has four neighboring fluorides in the yz plane of the octahedron at 2.010 ±0.015 A shown in Fig. 1(b) and two differently placed fluorides at 1.999±0.02 A along the x axis. Following Tinkham,[13] who first studied electron spin resonance of iron group elements in ZnF_2, we shall designate the four fluorides in the yz plane as type I and the two along the x axis as type II. Furthermore, it can be seen that the fluoride ion environment of a body-centered Ni^{++} ion differs from that of a corner Ni^{++} ion by a 90° rotation about the z axis, which in both cases coincides with the [001] crystallographic direction. Each fluoride ion is surrounded by three Ni^{++} ion near neighbors. One-half of the fluorides have their three neighbors in a $(1\bar{1}0)$ plane and the other half have their neighbors in a $(1\bar{1}0)$ plane, which of course is perpendicular to the first. It has been shown[1,14] that anisotropic interactions between fluoride ions and nickel ions will result in two different fluorine nuclear resonances for arbitrary directions of the external magnetic field H_0. However, for H_0 in the (100) or (010) planes only one resonance will be observed. When H_0 is along [110] and $[1\bar{1}0]$ it will coincide with the principal axes of the fluoride ions interactions with the nickel. The two different fluoride sites, however, will provide two different interactions, and it will be necessary to use additional information to decide which site is responsible for a particular interaction with the neighbors. This is discussed in more detail below, where the experimental results in the paramagnetic state, antiferromagnetic state, and transition region are presented separately.

RESONANCE SPECTROMETER

Two different nuclear magnetic resonance spectrometers were used during the experiments on NiF_2. One was a conventional Varian Associates V-4311 fixed-frequency induction spectrometer operating at 60.000 Mc/sec. Although this equipment was designed for use as a high-resolution spectrometer, it has several attractive features when used to observe the F^{19} resonance in paramagnetic salts. The high frequency affords high resolution of the F^{19} resonances in the paramagnetic state because the fluorine resonance shifts are proportional to H_0. In our experiments the shifts are megacycles rather than cycles but the resolution is still necessary because the lines are correspondingly broad. A second advantage of this spectrometer is the large value of rf field, which can be obtained at the sample without introducing additional noise. In our spectrometer the maximum value of rf field was $H_1=0.17$ gauss, where H_1 is one of the two rotating circularly polarized components of the rf field. This means that the linearly polarized component was 0.34 gauss maximum. This is about a factor of eight larger than the value of H_1 we obtain with marginal oscillators operating at their point of optimum signal-to-noise. Since the fluorine resonances are not saturated, the signal is proportional to H_1 and the large value was most helpful. A third attractive feature of this spectrometer is that the receiver coil is a plug-in unit so that for a given single crystal one can select a receiver coil to give the maximum filling factor. This spectrometer was used for all the 298°K measurements of the fluorine resonance.

The second spectrometer was a marginal oscillator whose frequency could be varied continuously from 20

[10] J. W. Stout (private communication).
[11] J. W. Stout and S. A. Reed, J. Am. Chem. Soc. **76**, 5279 (1954).
[12] W. H. Baur, Naturwiss. **44**, 349 (1957).
[13] M. Tinkham, Proc. Roy. Soc. (London) **A236**, 535, 549 (1956).
[14] N. Bloembergen and N. J. Poulis, Physica **16**, 915 (1950).

Mc/sec to 200 Mc/sec. This spectrometer was designed and built by H. R. Moore and H. Hopper at these Laboratories. In designing a spectrometer to cover this frequency range, our first approach was to try raising the upper frequency limit of a Pound-Knight-Watkins[15–17] type marginal oscillator. During the course of our efforts, Benedek informed us of the good performance of a push-pull marginal oscillator designed and built by Kushida which they were using to observe[18] the pressure dependence of the F^{19} nuclear resonance in antiferromagnetic[19] MnF_2 in the vicinity of 160 Mc/sec. The final form of the spectrometer used in our experiments follows the Kushida-Benedek model. The balanced line reduced shunt and stray capacity, and the circuit shown in Fig. 2 has been operating from 20–200 Mc/sec in a very sensitive fashion. The oscillator tube, a double triode Western Electric 396A, has the tuned circuit containing the sample connected to both grids. Away from the resonance frequency of the parallel tuned circuit the two grids are effectively shorted together so that push-pull oscillation only occurs at the parallel resonance frequency. The level of oscillation is regulated by the cathode bias level control. One important feature is the external rf amplifier, a Spencer-Kennedy chain amplifier model 202*D*, which gives 20-db gain from 100 kc/sec to 200 Mc/sec. This amplifier provides automatic level control by feedback to the oscillator grids, provides amplification of the rf signal for continuous frequency monitoring with a Hewlitt-Packard type 524*B* electronic counter and also after demodulation provides the audio envelope of the nuclear resonance. The demodulated output is also supplied to a microammeter through a dc cathode follower to monitor the rf level. The spectrometer sits directly on top of the double glass helium Dewar. Plug-in line stretchers allow one to keep the line approximately an odd integral multiple of $\lambda/2$. Plug-in shunt coils at the tube end of the line also help in the tuning, allowing selection of different frequency ranges. Different combinations of line and coil break up the range of 20–200 Mc/sec into seven separate regions. Continuous tuning within these overlapping regions is obtained by clock motor drive of either of two variable air condensers. A calibrator circuit, installed primarily to check sensitivity and allow proper adjustment of the audio lock-in phase, has also proved useful in cancelling amplitude modulation arising from frequency modulation. The best way of supplying frequency modulation was a back-biased silicon diode acting as a voltage sensitive capacitor. Mechanical shaking introduced by a mechanically varied condenser is eliminated by the junction diode. Magnetic field modulation has also been used with this spectrometer. One particularly valuable kind of magnetic field modulation for resonances observed in zero magnetic field is obtained by putting a germanium junction diode in series with a sine-wave modulation generator and the modulation coils. This automatically gives a half-wave rectified signal based on zero.

[15] R. V. Pound and W. D. Knight, Rev. Sci. Instr. **21**, 219 (1950).
[16] G. D. Watkins, thesis, Harvard University, 1952 (unpublished).
[17] J. M. Mays, H. R. Moore, and R. G. Shulman, Rev. Sci. Instr. **29**, 300 (1958).
[18] G. B. Benedek and T. Kushida, Phys. Rev. **118**, 46 (1960).
[19] V. Jaccarino and R. G. Shulman, Phys. Rev. **107**, 1196 (1957).

PARAMAGNETIC STATE MEASUREMENTS

Two single crystals were cut into approximately spherical shapes and mounted on sapphire rods. Both spheres were about 7 mm diameter. One crystal was mounted with its [001] axis parallel to the rod axis, so that the crystal could be rotated around [001] with $\mathbf{H}_0$ in the (001) plane. The other crystal was mounted with its [110] axis parallel to the rod. Upon rotating this rod $\mathbf{H}_0$ could be set parallel to [001] and [1$\bar{1}$0]. In Fig. 3 we have presented the results of rotating the crystal about the [001] direction while observing the resonance at a frequency of 60.0000 Mc/sec and $T=298°K$. At this frequency the normal F^{19} resonance field, ω/γ_N, is 14 979.4 gauss. The experiments show the resonances to be displaced to lower fields by several percent, the displacements being functions of the angle between $\mathbf{H}_0$ and the crystalline axes and also of the temperature and frequency. The two different F^{19} resonances observed with $\mathbf{H}_0 \| [110]$ correspond to the two different fluorine positions in the unit cell. As discussed previously[1] for MnF_2 where the pattern of experimental results at 298°K is the same (the only difference being the numerical values measured for the resonance shifts) for $\mathbf{H}_0$ in the {100} planes only one F^{19} resonance is expected in the paramagnetic state. For $\mathbf{H}_0$ in any other direction two fluorine resonances are expected. All our observations at $T=77°K$ and $T=298°K$ are in accord with these symmetry considerations. One of the main purposes of measuring these resonances in the paramagnetic state is to measure the hyperfine interaction between the fluorine nuclei and the magnetic electrons. The three principal axes for this interaction are labeled x, y, and z in Fig. 1(b). As can be seen from this illustration of the crystal structure, these axes coincide with the [001], [110], and [1$\bar{1}$0] crystalline directions. The two Ni^{++} ion sites differ from one another by a 90° rotation about the z or [001] axis. Because of this for a particular (110) plane one-half of the F^- have their three nearest Ni^{++} ions in the plane while the other half of the F^- ions have their three nearest Ni^{++} ions perpendicular to this plane. However, the three crystal directions [001], [110], and [1$\bar{1}$0] do coincide with three principal axes of the fluorine hyperfine interaction. Measurements of the nuclear resonance shifts with $\mathbf{H}_0$ along these three directions allow us to determine the three independent hyperfine interaction parameters which can be obtained from nuclear resonance studies in the paramagnetic state. For the purposes of analysis, the

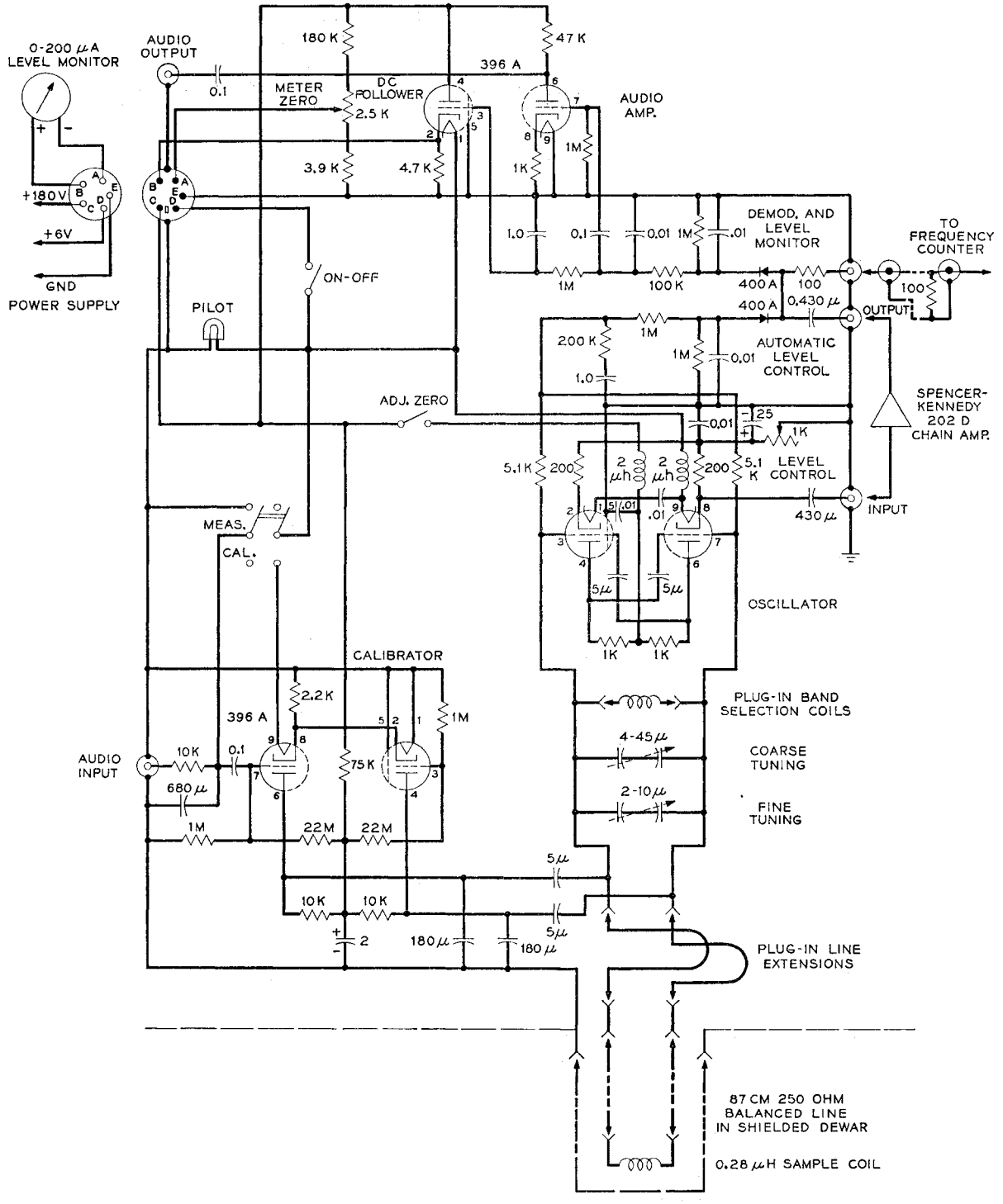

FIG. 2. Circuit diagram of variable frequency NMR spectrometer built by H. R. Moore and H. Hopper. All condensers are in units of 10^{-6} farad.

experimental results are conveniently represented by

$$\nu = (g_N\beta_N/h)(1+\alpha)H_0, \qquad (1)$$

where the different values of α are given in Table I for the different temperatures at which measurements have been made. This table contains the same information presented in Fig. 3, i.e., no corrections have been applied to the values of α calculated from Eq. (1).

ANALYSIS OF PARAMAGNETIC STATE RESONANCE SHIFTS

The Hamiltonian for the nuclear interactions in NiF_2 is

$$\mathcal{H}=-g_N\beta_N\mathbf{I}\cdot(\mathbf{H}_0+\mathbf{H}^D)+2\mathbf{S}^{\mathrm{I}}\cdot\mathbf{A}^{\mathrm{I}}\cdot\mathbf{I}+\mathbf{S}^{\mathrm{II}}\cdot\mathbf{A}^{\mathrm{II}}\cdot\mathbf{I}, \quad (2)$$

where $\mathbf{I}$ is the nuclear spin with g factor g_N, and β_N is the nuclear magneton. $\mathbf{H}_0$ is the external magnetic field, $\mathbf{S}^{\mathrm{I}}$ and $\mathbf{S}^{\mathrm{II}}$ the spins of Ni^{++} ions which are type I and type II neighbors of the fluoride ion in question and $\mathbf{A}^{\mathrm{I}}$ and $\mathbf{A}^{\mathrm{II}}$ the hyperfine interaction tensors with the two types of Ni^{++} ions. The dipole field of all i Ni^{++} atoms at the fluorine site is

$$\mathbf{H}^D=\sum_i\frac{3(\mathbf{r}_i\cdot\chi_i\cdot\mathbf{H})\mathbf{r}_i}{Nr_i^5}-\frac{\chi_i\cdot\mathbf{H}}{Nr_i^3}, \quad (3)$$

where $\mathbf{r}_i$ is the vector from the fluorine atom to the ith nickel ion, χ_i is the second-order tensor representing the molar susceptibility of a Ni^{++} ion, N is Avogadro's number, and $\mathbf{H}$ is the field at the Ni^{++} ion sites. In the paramagnetic region for our special samples, the error introduced by setting $\mathbf{H}=\mathbf{H}_0$ is negligible.

Writing this equation in terms of the nuclear resonance transitions observed for $\mathbf{H}_0$ along the principal axes, we have

$$g_N\beta_N\left(\alpha_{001}-\frac{H_{001}{}^D}{H_0}\right)=-\frac{1}{H_0}\langle S_z\rangle(2A_z{}^{\mathrm{I}}+A_z{}^{\mathrm{II}}), \quad (4)$$

$$g_N\beta_N\left(\alpha_{110}-\frac{H_{110}{}^D}{H_0}\right)=-\frac{1}{H_0}(2\langle S_y{}^{\mathrm{I}}\rangle A_y{}^{\mathrm{I}}+\langle S_x{}^{\mathrm{II}}\rangle A_x{}^{\mathrm{II}}), \quad (5)$$

$$g_N\beta_N\left(\alpha_{1\bar{1}0}-\frac{H_{1\bar{1}0}{}^D}{H_0}\right)=-\frac{1}{H_0}(2\langle S_x{}^{\mathrm{I}}\rangle A_x{}^{\mathrm{I}}+\langle S_y{}^{\mathrm{II}}\rangle A_y{}^{\mathrm{II}}), \quad (6)$$

where the α's represent the fractional resonance shift along the principal axes designated by their subscripts and listed in Table I and $\langle S_z\rangle$ is the expectation value of the zth component of spin with similar nomenclature for the x and y components. In these dense paramagnetic salts with large exchange interactions between the spins we cannot calculate $\langle\mathbf{S}\rangle$ from energy considerations as we could if the spins were independent. However, it can be related to the measured value of the susceptibility. The molar susceptibility is defined as

$$\chi_m=\sum_i^N\frac{\langle\mu_i\rangle}{H_0}, \quad (7)$$

where $\langle\mu_i\rangle$ is the expectation value of the moment of the ith site. The general expression for $\langle S_z\rangle$ including the high-frequency or temperature-independent contributions to the susceptibility has been shown to be[2]

$$\langle S_z\rangle=-\frac{[\chi_z-N\beta^2(2-g_z)/\lambda]}{Ng_z\beta}H_0, \quad (8)$$

where λ is the spin-orbit coupling whose value for Ni^{++} is -300 cm^{-1}, β is the Bohr magneton, and g_z is the electronic g factor in the z direction. Since $N\beta^2(2-g_z)/\lambda$ is the temperature-independent contribution to the susceptibility, it can be seen that one obtains $\langle S\rangle$ by subtracting the temperature-independent contributions from the measured susceptibility and including the temperature-dependent orbital contributions in the measured value of the g factor.

In order to determine the components of the tensor $\mathbf{A}$ in Eqs. (4)–(6), it is first necessary to measure the fractional shifts α of the resonances, with H_0 along the principal axes. As we will show in the next section, near the antiferromagnetic transition, which has been shown by specific heat measurements to be $T_N=73.2$°K, the susceptibility exhibits some unusual properties. To avoid these complications, we have decided to base our determinations of the A's upon the nuclear resonance shifts measured at 298°K. In addition to the measured values of α, it is necessary to have numerical values for the dipole sums of Eq. (3). Since off-diagonal contributions will be important in the antiferromagnetic state, we shall present the dipole sum in a general fashion and

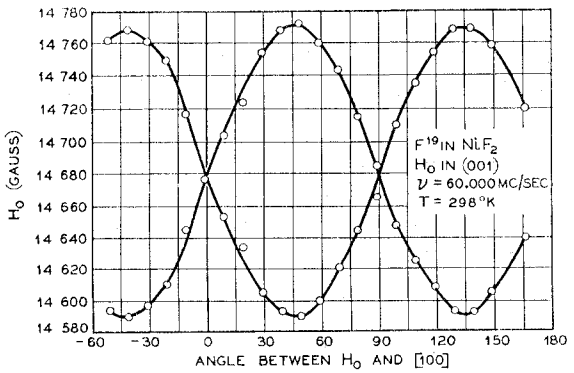

FIG. 3. Magnetic field required for resonance of the F^{19} nuclei as function of the angle between H_0 and [100] at a frequency of 60.0000 Mc/sec and at $T=298$°K.

TABLE I. Experimental values of $\alpha\equiv(\omega/\gamma_N-H_0)/H_0$ at different temperatures and orientations. The ratio of α to the temperature-dependent part of the susceptibility in the last column is seen to depend upon temperature for H_0 in (001).

Direction of $\mathbf{H}_0$	α in percent	Temperature °K	$\alpha\Big/\left[\chi_m-\frac{N\beta^2(2-g)}{\lambda}\right]$
[001]	2.247±0.02	298°	7.15
	4.187±0.01	90°	7.36
	4.292±0.01	77.3°	7.26
[110]	1.429±0.02	298°	4.42
	2.676±0.02		8.28
	2.36 ±0.03	90.3°	4.03
	4.95 ±0.03		8.46
	1.450±0.03	77.3°	2.39
	5.560±0.02		9.16

subsequently select the proper values for the particular directions used in Eqs. (4–6). The coordinates chosen are illustrated in Fig. 1(a). The dipole sum is performed over the coordinates of the tetragonal unit cell a, b, and c or [100], [010], and [001]. Consider the origin of this coordinate system at the lower left-hand corner nickel ion. We shall calculate the dipole sum at the fluorine located at u, u, 0. For generality we present this sum in terms of the separate contributions from the Ni^{++} ions at the corner position which we designate sublattice A and from the Ni^{++} ions at the body-centered position designated sublattice B. The sum is calculated on an IBM 704 to be

$$\mathbf{H}^D=\begin{pmatrix}0.0624 & 0.1582 & 0\\ 0.1582 & 0.0624 & 0\\ 0 & 0 & -0.1248\end{pmatrix}\begin{pmatrix}\langle\mu_a{}^A\rangle\\ \langle\mu_b{}^A\rangle\\ \langle\mu_c{}^A\rangle\end{pmatrix}+\begin{pmatrix}-0.0876 & 0.1334 & 0\\ 0.1334 & -0.0876 & 0\\ 0 & 0 & 0.1752\end{pmatrix}\begin{pmatrix}\langle\mu_a{}^B\rangle\\ \langle\mu_b{}^B\rangle\\ \langle\mu_c{}^B\rangle\end{pmatrix}, \quad (9)$$

where $\langle\mu_a{}^A\rangle$ is the component of the expectation value of the magnetic moment of the Ni^{++} ion on the A sublattice along the a or [100] direction, etc. The numbers are in units of 10^{24} cm^{-3}. In the paramagnetic state the directions of interest are [110], [1$\bar{1}$0], and [001] which are principal axes of the hyperfine interaction. These axes coincide with the right-handed x, y, and z axes of the individual Ni^{++} ions shown in Fig. 1(b) but not with the crystal axis of Fig. 1(a) and our dipole sum. We arbitrarily have set the [110] direction to coincide with the radius from Ni^{++} ion A to the F^- ion at $(u,u,0)$. For these directions we have the following components of μ in terms of the components at the individual sites:

$$\begin{aligned}
\langle\mu_a{}^A\rangle&=\frac{1}{\sqrt{2}}(\langle\mu_x{}^A\rangle-\langle\mu_y{}^A\rangle),\\
\langle\mu_a{}^B\rangle&=\frac{1}{\sqrt{2}}(\langle\mu_x{}^B\rangle+\langle\mu_y{}^B\rangle),\\
\langle\mu_b{}^A\rangle&=\frac{1}{\sqrt{2}}(\langle\mu_x{}^A\rangle+\langle\mu_y{}^A\rangle),\\
\langle\mu_b{}^B\rangle&=\frac{1}{\sqrt{2}}(-\langle\mu_x{}^B\rangle+\langle\mu_y{}^B\rangle),\\
\langle\mu_c{}^A\rangle&=\langle\mu_z{}^A\rangle,\\
\langle\mu_c{}^B\rangle&=\langle\mu_z{}^A\rangle.
\end{aligned} \quad (10)$$

The magnetic moments at the Ni^{++} ion sites are written in components along the x, y, and z axes of these sites. In the paramagnetic state these individual components can be related to the corresponding component of the molar susceptibility through Eq. (7). For the particular cases of $\mathbf{H}_0$ along the three principal axes, we have the following components of μ:

$$[110]\begin{cases}\langle\mu_x{}^A\rangle=(H_0/N)\chi_x,\\ \langle\mu_y{}^B\rangle=(H_0/N)\chi_y,\end{cases} \quad (11)$$

$$[1\bar{1}0]\begin{cases}\langle\mu_y{}^A\rangle=(H_0/N)\chi_y,\\ \langle\mu_x{}^B\rangle=-(H_0/N)\chi_x,\end{cases} \quad (12)$$

$$[001]\quad \langle\mu_z{}^A\rangle=\langle\mu_z{}^B\rangle=(H_0/N)\chi_z, \quad (13)$$

while all other components are zero. In the antiferromagnetic state, where spontaneous sublattice magnetizations exist, the nonvanishing components of magnetic moment are quite different and to a first approximation are independent of the external magnetic field. Substituting the values of Eqs. (11–13) into Eq. (9), we obtain the following values for the components of the dipole fields along H_0 in the paramagnetic state:

$$H_{110}{}^D=[0.366\chi_x+0.076\chi_y]H_0, \quad (14)$$

$$H_{1\bar{1}0}{}^D=[-0.159\chi_y-0.367\chi_x]H_0, \quad (15)$$

$$H_{001}{}^D=0.0837\chi_z H_0. \quad (16)$$

The differences between χ_x and χ_y can be calculated as follows. Using Moriya's[8] expression for the susceptibilities, we have

$$\chi_x=\frac{2Ng_x{}^2\beta^2}{3k(T+\Theta)}+\frac{N\beta^2(2-g_x)}{\lambda}, \quad (17)$$

with similar expressions for y and z. Of course, $\chi_\perp=(\chi_x+\chi_y)/2$ and $\chi_{\parallel}=\chi_z$, while Θ is the paramagnetic Curie point.

During the course of this investigation, it became evident that more accurate values of the susceptibility were required than previously available. Cooke and Lazenby[20] have measured $\chi_\perp$ in the paramagnetic region on one of our single crystals. Their measurements extend from 73.4°K to 287.4° and can be extrapolated accurately to 298°K where $\chi_\perp=3.53\times10^{-3}$ cm^3 mole^{-1}. This value has been corrected for diamagnetism by the addition of 32×10^{-6} per mole. We shall use this value of $\chi_\perp$ in preference to the value of $\chi_\perp=3.36\times10^{-3}$ cm^3 mole^{-1} obtained from the measurements of de Haas *et al.*[9] on powdered NiF_2 by use of the magnetic anisotropy values of Matarese and Stout[6] of $\chi_\perp-\chi_{\parallel}=0.1102\times10^{-3}$ cm^3 mole^{-1} at 301.5°K and $\chi_\perp-\chi_{\parallel}=0.1890\times10^{-3}$ cm^3 mole^{-1} at 90.07°K. The extrapolated value at 298°K is 0.110×10^{-3} cm^3 mole^{-1}, so that at this temperature $\chi_{\parallel}=3.42\times10^{-3}$ cm^3 mole^{-1}. Now it can be shown[2] by a perturbation treatment that

$$g_z=g_{av}+\tfrac{2}{3}D/\lambda=2.32\equiv g_3, \quad (18)$$

$$g_y=g_{av}-(\tfrac{1}{3}D-E)/\lambda=2.33\equiv g_1, \quad (19)$$

$$g_x=g_{av}-(\tfrac{1}{3}D+E)/\lambda=2.34\equiv g_2, \quad (20)$$

[20] A. H. Cooke and R. Lazenby (private communication).

in which g_1, g_2, and g_3 are the g factors as defined by Moriya and where we have taken $g_{av}=2.33$; $D=4.18$ cm^{-1} and $E=2.67$ cm^{-1} from Peter's[21] paramagnetic resonance data on Ni^{++} in ZnF_2. The various terms are defined by the spin Hamiltonian

$$\mathcal{H}=D(S_z^2-\tfrac{1}{3}S(S+1)]+E(S_x^2-S_y^2)+\beta\mathbf{H}\cdot\mathbf{g}\cdot\mathbf{S}. \quad (21)$$

The variations in the temperature-independent contribution to χ can be determined to be small. We can evaluate $N\beta^2(2-g_x)/\lambda=0.29\times10^{-3}$, and the corresponding expressions for y and z are 0.28×10^{-3} and 0.27×10^{-3}, all in units of cm^3 mole^{-1}. Since the first term of Eq. (17) predominates, $\chi_x/\chi_y\sim(g_x/g_y)^2=1.01$, or $\chi_x=1.005\chi_\perp$ and $\chi_y=0.995\chi_\perp$. Substituting these values in Eq. (8), we get

$$\langle S_z\rangle=-\frac{[3.42\times10^{-3}-0.27\times10^{-3}]}{6.03\times10^{23}\times0.927\times10^{-20}\times2.32}H_0$$
$$=-0.243\times10^{-6}H_0, \quad (22)$$

$$\langle S_y\rangle=-\frac{[3.51\times10^{-3}-0.28\times10^{-3}]}{6.03\times10^{23}\times0.927\times10^{-20}\times2.33}H_0$$
$$=-0.248\times10^{-6}H_0, \quad (23)$$

$$\langle S_x\rangle=-\frac{[3.55\times10^{-3}-0.29\times10^{-3}]}{6.03\times10^{23}\times0.927\times10^{-20}\times2.34}H_0$$
$$=-0.249\times10^{-6}H_0, \quad (24)$$

where the values of $\chi_x=3.55\times10^{-3}$ cm^3 mole^{-1} and $\chi_y=3.51\times10^{-3}$ cm^3 mole^{-1} have been used for 298°K. The experimental uncertainties in the value of $\chi_{298°}$ are greater than the differences of $\langle S\rangle$ for the different directions. The purpose in calculating these individual components so carefully was to keep the anisotropic part of the calculations as accurate as possible. However, since the uncertainty in the susceptibility is larger than the difference between $\langle S_x\rangle$ and $\langle S_y\rangle$ and since this makes the dipole correction uncertain, we shall ignore the differences and use $\langle S_x\rangle=\langle S_y\rangle=0.2485\times10^{-6}H_0$. Substituting these values along with those listed in Table I and Eqs. (14)–(16) into Eqs. (4)–(6) we obtain the following two alternative sets of values for the hyperfine interactions.

$$2A_z^{\mathrm{I}}+A_z^{\mathrm{II}}=121.7\times10^{-4}\text{ cm}^{-1},$$
$$2A_y^{\mathrm{I}}+A_x^{\mathrm{II}}=135.3\times10^{-4}\text{ cm}^{-1}, \quad (25)$$
$$2A_x^{\mathrm{I}}+A_y^{\mathrm{II}}=86.8\times10^{-4}\text{ cm}^{-1},$$

or

$$2A_z^{\mathrm{I}}+A_z^{\mathrm{II}}=121.7\times10^{-4}\text{ cm}^{-1},$$
$$2A_y^{\mathrm{I}}+A_x^{\mathrm{II}}=68.3\times10^{-4}\text{ cm}^{-1}, \quad (26)$$
$$2A_y^{\mathrm{I}}+A_y^{\mathrm{II}}=153.7\times10^{-4}\text{ cm}^{-1}.$$

[21] M. Peter and J. B. Mock, Phys. Rev. **118**, 137 (1960).

The alternative sets of values for the x and y combinations result from the impossibility of deciding *a priori* which resonance line is caused by a particular hyperfine interaction. The dipole contributions to a fluorine position only depend upon the position of $\mathbf{H}_0$ *with respect to that site.* However, there are two different fluorine positions which differ from each other by a 90° rotation about the [001] axis. Once $\mathbf{H}_0$ is fixed with respect to a particular fluoride ion site, then the particular hyperfine interactions of that site are fixed. This means that if we tentatively identify one of the observed resonances as being due to a particular hyperfine interaction, i.e., $2A_x^{\mathrm{I}}+2A_y^{\mathrm{II}}$, then the dipole correction to that shift α is fixed as $H_{[1\bar{1}0]}{}^D$ using the conventions of Fig. 1. When we consider the possibility that the other resonance may be from the same combination of hyperfine interactions, then its dipole correction is the same. In Appendix A, Eq. (25) is shown to be the correct alternative by considering the atomic origin of the hyperfine interaction. Tinkham[13] has written the hyperfine interaction for the rutile lattice in the form

$$A_i{}^N=A_s{}^N+(A_\sigma{}^N-A_{\pi'}{}^N)(3\cos^2\theta_{i,\sigma}-1)$$
$$+(A_\pi{}^N-A_{\pi'}{}^N)(3\cos^2\theta_{i,\pi}-1), \quad (27)$$

where $i=x$, y, or z; $N=$I or II for type I or type II bonds, and the isotropic interaction is $A_s{}^N$. The anisotropic hyperfine interactions measured represent the differences between spin density along two directions and the third. Isotropic interactions are associated with unpaired spins with s electron character and anisotropic interactions with p electrons. The directional properties depend upon the angle between the spin density and the external magnetic field. This angle is designated $\theta_{i,\sigma}$ and $\theta_{i,\pi}$ for H_0 along the ith axis and the unpaired spins along the σ or π bond direction. In the notation of Eq. (27) the π axis is chosen perpendicular to the plane containing a fluoride ion and its three nearest neighbor nickel ions. Both the σ and π' directions lie in this plane, and in Tinkham's considerations the σ direction coincides with the fluorine-nickel internuclear radius. This, of course, is the usual definition of σ bonding, i.e., no angular momentum about the internuclear radius. However, it has been mentioned[22] that the d orbitals as split by the cubic crystal field into a doublet and triplet are not arranged so as to have the directions of greatest electron density coincide with the directions of the fluoride ligands in the yz plane. Rather, the d electrons make right angles with each other in this plane (being z^2-y^2 in their directional dependence) while the F−Ni^{++}−F angle bisected by the z axis is 79.8° in NiF_2. Of course, by hybridization it is possible to create linear combinations of z^2-y^2 and yz with the same orthorhombic symmetry as the ligands. However, the energy required for promotion and hybridization will only be available when the bonds

[22] A. M. Clogston, J. P. Gordon, V. Jaccarino, M. Peter, and L. R. Walker, Phys. Rev. **117**, 1222 (1960).

formed are strong and comparable with the crystal field splitting so that they provide enough energy to stabilize the hybridized configuration. Since our measurements indicate a small degree of covalent character, the hybridized configuration should be negligible. This same conclusion was reached by Keffer *et al.*[23] for the fluorine orbitals, where they showed that hybridization of the fluorine orbitals would give results inconsistent with the measurements made of separate bond interactions by paramagnetic resonance studies of Mn^{++} in ZnF_2. We shall disregard the small departure from octahedral symmetry required of the orbitals for the moment and calculate the atomic origin of the hyperfine interactions as if the σ bonds pointing along the internuclear radius include only the e_g orbitals of the metal ion, and the π interactions only the t_{2g} orbitals. Both of these classifications refer to the levels found after splitting by a cubic field. Under this assumption, Eq. (27) is considerably simplified. The $3d^8$ configuration of Ni^{++} means that in a cubic field only the e_g orbitals have unpaired electrons and only the σ bonds will have nonvanishing values of hyperfine interaction. Therefore, we put $A_\pi{}^N = A_{\pi'}{}^N = 0$ for $N = \mathrm{I}$ and II and Eq. (27) becomes in component form

$$\begin{aligned} A_x{}^{\mathrm{I}} &= A_s{}^{\mathrm{I}} - 1.000 A_\sigma{}^{\mathrm{I}}, \\ A_x{}^{\mathrm{II}} &= A_s{}^{\mathrm{II}} + 2.000 A_\sigma{}^{\mathrm{II}}, \\ A_y{}^{\mathrm{I}} &= A_s{}^{\mathrm{I}} + (3\cos^2\theta_{y,\sigma} - 1) A_\sigma{}^{\mathrm{I}}, \\ A_y{}^{\mathrm{II}} &= A_s{}^{\mathrm{II}} - 1.000 A_\sigma{}^{\mathrm{II}}, \\ A_z{}^{\mathrm{I}} &= A_s{}^{\mathrm{I}} + (3\sin^2\theta_{y,\sigma} - 1) A_\sigma{}^{\mathrm{I}}, \\ A_z{}^{\mathrm{II}} &= A_s{}^{\mathrm{II}} - 1.000 A_\sigma{}^{\mathrm{II}}, \end{aligned} \tag{28}$$

where $\theta_{y,\sigma}$ is the angle between the y axis and the unpaired spin in the fluorine p_σ orbital. Departures from octahedral symmetry are included in the calculations in Appendix A by allowing this angle to be an experimental parameter. The four components of A plus the angle require five experimental determinations. As discussed in Appendix A, we have included two measurements from the antiferromagnetic state. From these data the best fit is obtained for the following values of the hyperfine interaction in units of 10^{-4} cm^{-1}:

$$\begin{aligned} &A_s{}^{\mathrm{I}} = 36.4 \pm 1.8, \quad A_\sigma{}^{\mathrm{I}} = 9.1 \pm 0.9, \\ &A_s{}^{\mathrm{II}} = 42.1 \pm 2.1, \quad A_\sigma{}^{\mathrm{II}} = 9.9 \pm 0.9, \\ &\theta_{y,\sigma} = 54.0^\circ. \end{aligned} \tag{29}$$

The angle $\theta_{y,\sigma} = 54.0^\circ$ differs slightly from the structural angle between the y axis and the σ bond which is 50.1°. We shall include all departures from the O_h symmetry in this parameter, so that it is only necessary to discuss the σ bonds formed by the $d\gamma$ electrons and it is possible to neglect any unpaired spins in π bonds.

[23] F. Keffer, T. Oguchi, W. O'Sullivan, and J. Yamashita, Phys. Rev. **115**, 1553 (1959).

THE IONIC BOND

The hyperfine interactions measured can be converted into unpaired spin density in fluoride ion orbitals. The method followed has been to compare the measured hyperfine interactions with those expected when an unpaired spin is in a $2s$ or $2p$ state of the fluoride ion. The ratio of the hyperfine interactions (corrected to the same value of spin) then gives the fractional occupancy of fluoride ion orbitals. These relations are

$$\begin{aligned} f_s{}^N &= 2S A_s{}^N / A_{2s} = 2S A_s{}^N / 1.57, \\ f_\sigma{}^N &= 2S A_\sigma{}^N / A_{2p} = 2S A_\sigma{}^N / 0.044, \end{aligned} \tag{30}$$

in which $f_s{}^N$ and $f_\sigma{}^N$ are, respectively, the fraction unpaired $2s$ and $2p$ electrons on the fluoride from one bond of type $N = 1$ or 2. The hyperfine interactions of $2s$ and $2p$ electrons are represented by A_{2s} and A_{2p} and the numerical values (in units of cm^{-1}) have been derived from calculations by Hartree[24] and by Barnes and Smith.[25,26]

As mentioned previously,[13] these measurements can only determine the difference in occupancy of two of the fluorine p orbitals as compared with the third. In MnF_2 the ${}^6S_{\frac{5}{2}}$ state of the Mn^{++} ion described for the $3d^5$ configuration a half-filled shell of d electrons equally capable of forming bonds with the fluoride ion p orbitals pointing towards the manganese (the p_σ bonds), and with p orbitals not directed along the internuclear radius (the p_π bonds). In NiF_2 the $3d^8$ configuration of the nickel ion in the approximately octahedral field means that the two unpaired spins are essentially confined to the $d\gamma$ orbitals which can only form σ bonds with the fluoride ions. In Appendix A the small departures from this approximation because the nickel site has orthohombic symmetry are included in the variable $\theta_{y,\sigma}$. These effects are included in the possible errors listed in Eq. (29). In MnF_2 we were only able to determine that the difference in occupancy of the p_σ and p_π orbitals was a small number as shown in Table II. In NiF_2 the values shown in Table II come from the best-fit values of Eq. (29). The large amount of p_σ bonding is outstanding, particularly when compared with the

TABLE II. Comparison of the percent unpaired $2s$ and $2p$ character between MnF_2 and NiF_2. All values are in percent unpaired electron arising from each bond. The large amount of p_σ character in NiF_2 indicates that the small value of $f_\sigma - f_\pi$ in MnF_2 arose from the cancellation of p_σ by p_π.

	MnF_2	NiF_2	$KNiF_3$
$f_s{}^{\mathrm{I}}$	0.49±0.02	0.46±0.02	0.50±0.04
$f_s{}^{\mathrm{II}}$	0.52±0.02	0.53±0.03	
$f_\sigma{}^{\mathrm{I}} - f_\pi{}^{\mathrm{I}}$	0.2 ±0.3		
$f_\sigma{}^{\mathrm{II}} - f_\pi{}^{\mathrm{II}}$	0.4 ±0.3		
$f_\sigma{}^{\mathrm{I}}$		4.1 ±0.4	4.9 ±0.6
$f_\sigma{}^{\mathrm{II}}$		4.5 ±0.4	

[24] D. R. Hartree, Proc. Roy. Soc. (London) **151**, 96 (1935).
[25] R. G. Barnes and W. V. Smith, Phys. Rev. **93**, 95 (1954).
[26] T. Moriya, Progr. Theoret. Phys. (Kyoto) **16**, 23, 641 (1956).

small amount of $p_\sigma - p_\pi$ bonding in MnF_2. The inescapable conclusion is that p_π bonding, when allowed, is much larger than previously considered, and is, in fact, almost as important as the p_σ bonding. This has been discussed more completely in our report[27] on the bonding in $KNiF_3$ and K_2NaCrF_6 where the O_h symmetry of the metal ions simplified the discussion.

PARAMAGNETIC STATE LINEWIDTHS

In the paramagnetic region the linewidths were measured with H_0 along the three principal directions of the hyperfine interaction at 298°K and 77.3°K. The lines were Lorentzian in shape while the intervals between extrema of absorption derivatives, δH, which depended somewhat upon temperature, are listed in Table III. Converting these widths into T_2 by the relation $1/T_2 = (\sqrt{3}/2)\gamma\delta H$, we have the values listed in column three of Table III. Moriya[26] has calculated the widths expected for exchange narrowed nuclear resonance lines and this mechanism has been shown[2,3] to be responsible for linewidths in other paramagnetic salts. The equation for the spin-spin relaxation time T_2 is

$$\frac{1}{T_2} = \left(\frac{\pi}{2}\right)^{\frac{1}{2}} \frac{S(S+1)}{3\hbar^2\omega_e} \sum_i (\cos^2\theta_i + \tfrac{1}{2}\sin^2\theta_i) B_i^2, \quad (31)$$

where S is the electron spin, θ_i is the angle between the ith principal axis of the hyperfine interactions and the direction of the external magnetic field, and B_i is the ith component of the magnetic interaction between electrons and the fluorine nuclei. The electronic exchange frequency is ω_e. Since the nuclei react the same regardless of whether the origin of the interaction is hyperfine or dipolar, it is necessary to include both contributions in B_i. The most straightforward way of calculating these values of B_i is to ignore the dipole corrections in Eqs. (4)–(6). Doing this and substituting the values in Eq. (31), we obtain theoretical relative widths without knowing ω_e. These relative widths are

$$\left.\frac{1}{T_2}\right|_{2A_z^{\mathrm{I}}+A_z^{\mathrm{II}}} = 0.91 \left.\frac{1}{T_2}\right|_{2A_y^{\mathrm{I}}+A_x^{\mathrm{II}}} = 1.19 \left.\frac{1}{T_2}\right|_{2A_x^{\mathrm{I}}+A_y^{\mathrm{II}}}, \quad (32)$$

while the experimental results at 298°K are

$$\left.\frac{1}{T_2}\right|_{2A_z^{\mathrm{I}}+A_z^{\mathrm{II}}} = 0.85 \left.\frac{1}{T_2}\right|_{2A_y^{\mathrm{I}}+A_x^{\mathrm{II}}} = 1.09 \left.\frac{1}{T_2}\right|_{2A_x^{\mathrm{I}}+A_y^{\mathrm{II}}}. \quad (33)$$

TABLE III. Linewidth of the F^{19} resonance in the paramagnetic state.

Hyperfine interaction	Temperature (°K)	T_2 (seconds $\times 10^{-6}$)	δH (gauss)
$2A_z^{\mathrm{I}}+A_z^{\mathrm{II}}$	298	1.88	24.2±1
$2A_z^{\mathrm{I}}+A_z^{\mathrm{II}}$	77	2.54	17.9±1
$2A_y^{\mathrm{I}}+A_x^{\mathrm{II}}$	298	1.61	28.3±1
$2A_y^{\mathrm{I}}+A_x^{\mathrm{II}}$	77	2.68	17.0±1
$2A_x^{\mathrm{I}}+A_y^{\mathrm{II}}$	298	2.05	22.2±1
$2A_x^{\mathrm{I}}+A_y^{\mathrm{II}}$	77	3.16	14.4±1

[27] R. G. Shulman and K. Knox, Phys. Rev. Letters 4, 603 (1960).

TABLE IV. Comparison between the exchange frequency, ω_e, calculated from nuclear resonance linewidths and from the Néel temperature in transition element fluorides. Units are 10^{12} radians/sec.

	NiF_2	MnF_2	$KMnF_3$
ω_e (Linewidth)	16	7.0	6.2
ω_e (Néel temperature)	9.3	4.3	6.6
ω_e (Antiferromagnetic resonance)		7.0	

These experimental ratios at 298°K agree with theory when the experimental accuracy of ±1.5 gauss is included, introducing a ten percent error in the ratios. However, calculating ω_e from the $2A_z^{\mathrm{I}}+A_z^{\mathrm{II}}$ line we find $\omega_e = 1.6\times 10^{13}$ sec^{-1} while calculating it from[28]

$$\omega_e = \frac{k\Theta}{\hbar}\left(\frac{6}{zS(S+1)}\right)^{\frac{1}{2}}, \quad (34)$$

where z is the number of neighboring nickel ions on the opposite sublattice and Θ is defined by $\chi = C/(T+\Theta)$. We find $\omega_e = 9.3\times 10^{12}$ sec^{-1}, which is too small by a factor of 1.7. In MnF_2, calculations of the anisotropy field[29] and antiferromagnetic resonance measurements[30] could be combined to give a value of ω_e which was in perfect agreement[1] with experiment, namely, $\omega_e = 7.0 \times 10^{12}$ sec^{-1}. If we calculate ω_e from Eq. (34) for MnF_2, we find it to be 4.3×10^{12} which is again too small by a factor of 1.6. In Table IV we have listed the values of ω_e calculated from the exchange narrowing formula and from the molecular field approximation for the nickel and manganese compounds which we have reported. It can be seen that the exchange narrowing gives a larger value of ω_e than does the molecular field. A possible cause of this difference is that exchange interactions contributing to the magnetic ordering are responsive to the sign of the interaction so that the near neighbors along [001] tend to cancel the other sublattice, whereas all exchange interactions narrow the nuclear resonance line. If this is the only explanation of the discrepancy, the rather large factors of 1.6 between the two values of ω_e would indicate very large contributions from the nearest neighbors.

ANTIFERROMAGNETIC REGION

When we started this study, it was known from susceptibility[6] and specific heat[5] measurements, coupled with a neutron diffraction[7] investigation, that NiF_2 became antiferromagnetic at 73.2°K. A chronological description of our first experiments on NiF_2 in the antiferromagnetic state might clarify some of the unusual features of this state. Our original plan for at-

[28] T. Nagamiya, K. Yosida, and R. Kubo, *Advances in Physics*, edited by N. F. Mott (Taylor and Francis, Ltd., London, 1955), Vol. 4, p. 1.
[29] F. Keffer, Phys. Rev. **87**, 608 (1952).
[30] F. M. Johnson and A. H. Nethercot, Jr., Phys. Rev. **104**, 847 (1956).

tacking the antiferromagnetic state of NiF_2 was similar to the approach previously taken in MnF_2,[19] FeF_2,[31] and CoF_2.[31] From the measurements in the paramagnetic region the hyperfine interaction constants could be determined as has been done for NiF_2 in the last section. With the values of the hyperfine interaction, it had been shown[19,32] that it was possible to predict the nuclear resonance frequency in the antiferromagnetic state by the expression

$$\nu=\frac{1}{h}[2\mathbf{A}^{\mathrm{I}}\cdot\mathbf{S}^{\mathrm{I}}-\mathbf{A}^{\mathrm{II}}\cdot\mathbf{S}^{\mathrm{II}}][\beta]\frac{M(T)}{M(0)}+\frac{\gamma_N}{2\pi}[H_0+H^D], \quad (35)$$

where the degree of alignment in the antiferromagnetic state at $T=0$ is[33]

$$\beta=1-\frac{zS}{(2zS-1)^2}, \quad (36)$$

where z is the number of near neighbors. For NiF_2, $\beta=0.964$. The sublattice magnetization at any temperature T is $M(T)$ while the dipole field $\mathbf{H}^D$ given by Eq. (9) is also a function of sublattice magnetization. In our discussion we shall ignore any dependence of the hyperfine interaction $\mathbf{A}$ upon the temperature (one obvious origin of this would be the thermal expansion of the lattice). Compared to the paramagnetic state where, as shown in Eqs. (22)–(24), $\langle S\rangle=0.247\times10^{-6}H_0=0.35\times10^{-3}$ for $H_0=14\times10^3$, in the antiferromagnetic state $|S|$ (β) is close to unity. This shows that in the antiferromagnetic state, where the expectation value of the individual spin is essentially the absolute magnitude of the spin, the time-averaged fields at the nuclei approach the instantaneous fields which are very large. The nuclear resonance frequency predicted depends markedly upon the direction of the spin alignment because of the anisotropic nature of the hyperfine interactions and dipole fields. The neutron diffraction[7] data available at the beginning of this investigation indicated that the c axis was the direction of spin alignment for the two sublattices with a tipping of a few degrees towards the ab plane. If we ignore the tipping and consider the spins along the c axis, then substituting the best values of the A's obtained from the paramagnetic state measurements into Eq. (35), we find that for $H_0=0$, $\nu\cong200$ Mc/sec with the internal field along the [001] direction.

However, the fluorine resonance was found in a completely different frequency region. It was first observed with the 60.000-Mc/sec fixed-frequency Varian induction spectrometer at 20.3°K with $H_0\|[001]$, where the external magnetic field was $\sim11{,}000$ gauss. Obviously these conditions were not created until a number of more likely experiments had been tried. Since the 11 000 gauss corresponded to ~44 Mc/sec, then upon the assumption that the internal field was also parallel to [001], we searched at zero field with the variable-frequency spectrometer in the region of 104 Mc/sec and 16 Mc/sec but without success. Although we were not able to observe the F^{19} resonance in zero external field with the variable-frequency spectrometer, we were able at $T=4.2$°K to observe the resonance at 48 Mc/sec and $H_0\cong7000$ gauss. As will be shown below, by measuring the magnetic field strength required for resonance at two different frequencies, it is possible by the law of cosines to calculate the strength of the internal field and the angle it makes with the external field. When this was done with $H_0\|[001]$, it was found that the angle between [001] and the internal field was 90°. At the same time, Moriya[8] had concluded from his analysis of the torque measurements that the direction of antiferromagnetic ordering was essentially [100], not [001]. At this point we shall discontinue the chronological description of the experiments and go to a discussion based upon the separate measurements made and their interpretation.

The direction and magnitude of the internal magnetic field at the fluorine nucleus were determined by a series of measurements made of resonance frequency vs external magnetic field. To the extent that the internal magnetic field, H_i, is independent of the external magnetic field H_0, the magnitude of H_i and its angle relative to H_0 can be calculated by the law of cosines. For the sake of simplicity we have kept $H_0\|[100]$ in these measurements so that only one line was observed. (It will be shown that for other orientations two resonances were observed.) Then if we picture the vectorial addi-

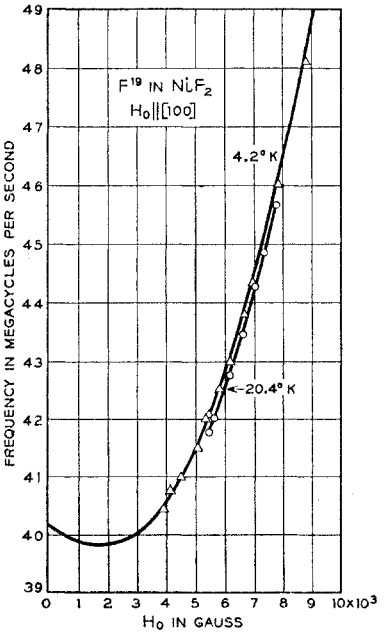

FIG. 4. Measurements of H_0 vs frequency with $H_0\|[100]$ at $T=20.3$°K and $T=4.2$°K. The solid lines are best fits of the law of cosines.

[31] V. Jaccarino, R. G. Shulman, J. Davis, and J. W. Stout, Bull. Am. Phys. Soc. 4, 41 (1958).
[32] B. Bleaney, Phys. Rev. **104**, 1190 (1956).
[33] J. C. Fisher, Bull. Am. Phys. Soc. 4, 53 (1959).

tion of H_0 and H_i, we have

$$(\omega/\gamma_N)^2=H_0^2+H_i^2+2H_0H_i\cos\varphi_i, \tag{36}$$

where φ_i is the angle between H_0 and H_i. The measurements made at 4.2°K and 20.3°K are shown in Fig. 4. We shall consider the data of 4.2°K. By taking these points in pairs it is possible to solve for φ_i and H_i. As a result of choosing seven pairs, we determined that $H_i=10\,075$ gauss and $\varphi_i=101.3°$. We shall not attach limits of error at this time but only say that the average deviations were 27 gauss and 0.2°, respectively. The angle of 101.3° indicates that for H_0 along a [100] axis H_i has a component which points in the opposite direction from H_0.

In another series of experiments a single crystal was mounted with $H_0\|[001]$ and at 4.2°K similar measurements were made of H_0 vs resonance frequency. Both sets of data are shown in Table V. If we take several pairs of these measurements with $H_0\|[001]$, we determine that for this orientation of H_0, $\varphi_i=90°$ and $H_i=10\,070$ gauss, where the average deviation in the angle is 0.5° and in the field is 25 gauss. Both sets of data will be analyzed more carefully below but the consequences at this point are inescapable. The internal field H_i lies in the (001) or *ab* plane and is about 101.3° away from the [100] or [010] direction along which H_0 is directed. These results are in good qualitative agreement with the model[8] of spin alignment in which the spins lie in the *ab* plane as shown in Fig. 5. They clearly show that Ericson's model is wrong since there is no component of H_i perpendicular to the (001) plane as his model requires. In Moriya's model, two different sublattices of Ni^{++} ions exist of which the *B* sublattice is at the body-centered position and the *A* sublattice at the corners. The spins are approximately antiparallel along the *a* or *b* directions. They are not perfectly antiparallel, however, being rotated from this axis by a small angle so as to create a small ferromagnetic component perpendicular to the direction of antiferromagnetic alignment. In order to compare the proposed spin alignment with the experimental observed fields at the fluorine nuclei,

TABLE V. Measurements of frequency vs H_0 at $T=4.2$°K or 20.3°K for the two cases of $H_0\|[100]$ and $H_0\|[001]$.

$H_0\|[100]$; $T=4.2$°K		$H_0\|[001]$; $T=20.3$°K	
ν (Mc/sec)	H_0 (gauss)	ν (Mc/sec)	H_0 (gauss)
49.900	9539	56.375	9826
48.126	8808	56.209	9767
46.040	7852	55.864	9643
44.355	6985	55.611	9559
43.810	6676	55.061	9371
43.012	6182		
42.520	5848		
42.060	5511		
41.966	5428		
41.514	5063		
41.000	4584		
40.748	4203		
40.452	3928		

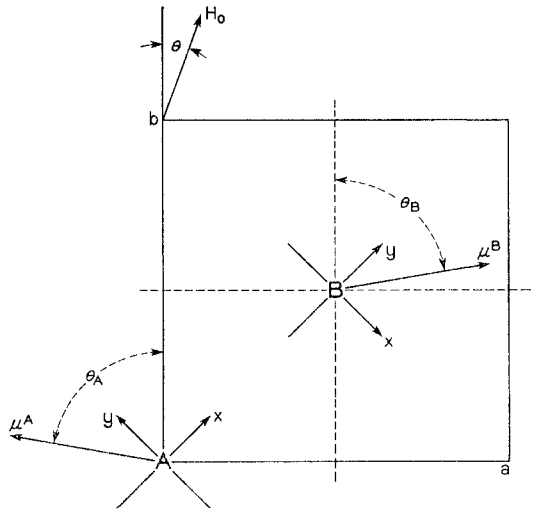

FIG. 5. Model of spin ordering in NiF_2 proposed by Moriya and confirmed by these measurements.

it is necessary to have a quantitative expression for the spin alignment as a function of H_0. In Fig. 5 the direction of the spins is shown for H_0 and the ferromagnetic moment along a [100] direction is designated as the *b* axis. The angles between the *b* axis and μ_A and μ_B are labeled θ_A and θ_B, respectively, and we define

$$\begin{aligned}\varphi&=\theta_B-\theta_A\equiv\pi-\eta,\\ \xi&\equiv(\theta_B+\theta_A)/2,\end{aligned} \tag{37}$$

where η is the total departure of the spins from being perfectly antiparallel and ξ is one half of the angle between the ferromagnetic component and the [100] direction. Both η and ξ are very small angles. The external magnetic field is considered to be in the (001) plane, making an angle θ with the *b* axis. From the spin Hamiltonian approach, Moriya[8] has shown that

$$\begin{aligned}\xi&=(\beta/8\alpha)\sin\theta+\cdots,\\ \eta&=2\alpha+\beta\cos\theta,\end{aligned} \tag{38}$$

where by using the numerical values discussed above we have

$$\alpha\equiv\frac{E}{JZ}=\frac{2.67\text{ cm}^{-1}}{95\text{ cm}^{-1}}=0.028,$$

$$\beta\equiv\frac{g\mu_BH_0}{JSZ}=\frac{2.16\times10^{-20}H_0}{1.89\times10^{-14}}=1.14\times10^{-6}H_0.$$

We shall compare the internal fields computed from this model with those calculated from the data of Table V for $H_0\|b$, or $\theta=0$. Under these conditions $\xi=0$ and

$$\tfrac{1}{2}(\theta_B-\theta_A)=\tfrac{1}{2}\pi-(\alpha+\tfrac{1}{2}\beta)=[\tfrac{1}{2}\pi-(0.028+0.57\times10^{-6}H_0)](180°/\pi). \tag{39}$$

For the antiferromagnetic ordering along the *a* axis of

TABLE VI. Values of θ_B as a function of H_0 for H_0 along the b axis, and the calculated values of the dipole fields along a and b.

H_0	θ_B	H_b	H_a
0	88.40	−530.2	−2952
4000	88.28	−531.4	−2939
5000	88.24	−531.9	−2934
6000	88.20	−532.1	−2931
7000	88.17	−532.5	−2927
8000	88.14	−532.7	−2923
9000	88.10	−533.1	−2920
10 000	88.07	−533.3	−2917

Fig. 5, the values of the magnetic moments at the sites are

$$\begin{aligned} &\langle\mu_a{}^A\rangle=-\sin\theta_B|\mu^A|, \quad \langle\mu_a{}^B\rangle=\sin\theta_B|\mu^B|,\\ &\langle\mu_b{}^A\rangle=\cos\theta_B|\mu^A|, \quad \langle\mu_b{}^B\rangle=\cos\theta_B|\mu^B|, \qquad (40)\\ &\langle\mu_c{}^A\rangle=0, \qquad\qquad \langle\mu_c{}^B\rangle=0, \end{aligned}$$

in which we have set $\theta_B=-\theta_A$. Table VI gives the values of θ_B for different values of H_0. The value of $\sin\theta_B$ is 0.9995 and changes negligibly over this range of H_0. The dipole fields have been calculated by substituting the values of Eq. (40) into Eq. (9), from which we obtain the following components of $\mathbf{H}^D$ along a, b, and c from sublattices A and B, respectively:

$$\begin{aligned} \mathbf{H}^D=&\begin{bmatrix} 0.0624 & 0.1582 & 0 \\ 0.1582 & 0.0624 & 0 \\ 0 & 0 & -0.1248 \end{bmatrix}\begin{bmatrix} -0.9995 \\ +\cos\theta_B \\ 0 \end{bmatrix}\\ &+\begin{bmatrix} -0.0876 & 0.1334 & 0 \\ 0.1334 & -0.0876 & 0 \\ 0 & 0 & +0.1752 \end{bmatrix}\begin{bmatrix} 0.9995 \\ +\cos\theta_B \\ 0 \end{bmatrix}\\ &\times 10^{24}\langle\mu\rangle, \qquad (41) \end{aligned}$$

or

$$\mathbf{H}^D=\begin{bmatrix} -0.1500 & +0.2915\cos\theta_B \\ -0.0248 & -0.0252\cos\theta_B \\ & 0 \end{bmatrix}\langle\mu\rangle\times 10^{24}\,\text{gauss}. \qquad (42)$$

Now the total moment of Ni^{++} in this crystal, including orbital contributions, is $g\beta S=2.16\times10^{-20}$ erg/gauss, plus a small temperature-independent contribution which can be neglected in the antiferromagnetic region. It is necessary to assume a degree of alignment of each sublattice and, as mentioned above, we shall follow Fischer's[33] calculation of $\beta=0.964$. This gives $\langle\mu'\rangle=2.08\times10^{-20}$ erg/gauss. The components of the dipole fields along a and b calculated from Eq. (42) are presented in the last two columns of Table VI. It is noteworthy that by aligning the ferromagnetic components along the positive b axis there is a net dipole field at the fluorine sites which is *negative* or opposed to the ferromagnetic moment and to H_0. Another interesting point is that, although decreasing the angle φ by increasing H_0 changes μ_b more than μ_a, still the off-diagonal terms in the dipole sum change the field component along a more than along b.

Using the same model of spin alignments we shall calculate the contributions of the hyperfine interactions to the internal magnetic field at the fluorine nuclei. For the fluorine site which we have considered at $(u,u,0)$, the type I hyperfine interactions are with the B sublattice of Ni^{++} ions at the body-centered position in Fig. 1(a) and the type II interaction with the A sublattice of Ni^{++} ions at the origin. Referring to Eq. (10), we now transform the spins into their components along the x, y, and z directions and have, using $\mu=-g\beta S$ and setting $B\equiv$I and $A\equiv$II,

$$\begin{aligned} &S_x{}^{\mathrm{II}}=\frac{1}{\sqrt{2}}(S_a{}^{\mathrm{II}}+S_b{}^{\mathrm{II}}), \qquad S_x{}^{\mathrm{I}}=\frac{1}{\sqrt{2}}(S_a{}^{\mathrm{I}}-S_b{}^{\mathrm{I}}),\\ &S_y{}^{\mathrm{II}}=\frac{1}{\sqrt{2}}(-S_a{}^{\mathrm{II}}+S_b{}^{\mathrm{II}}), \quad S_y{}^{\mathrm{I}}=\frac{1}{\sqrt{2}}(S_a{}^{\mathrm{I}}+S_b{}^{\mathrm{I}}), \qquad (43)\\ &S_z{}^{\mathrm{II}}=S_c{}^{\mathrm{II}}, \qquad\qquad S_z{}^{\mathrm{I}}=S_c{}^{\mathrm{I}}. \end{aligned}$$

Writing the hyperfine interactions out in terms of the tensor $\mathbf{A}$, we have

$$\begin{aligned} \textstyle\sum_N \mathbf{A}^N\cdot\mathbf{S}=&2\begin{pmatrix} A_{xx}{}^{\mathrm{I}} & 0 & 0 \\ 0 & A_{yy}{}^{\mathrm{I}} & \pm A_{yz}{}^{\mathrm{I}} \\ 0 & \pm A_{zy}{}^{\mathrm{I}} & A_{zz}{}^{\mathrm{I}} \end{pmatrix}\begin{pmatrix} S_x{}^{\mathrm{I}} \\ S_y{}^{\mathrm{I}} \\ S_z{}^{\mathrm{I}} \end{pmatrix}\\ &+\begin{pmatrix} A_{xx}{}^{\mathrm{II}} & 0 & 0 \\ 0 & A_{yy}{}^{\mathrm{II}} & 0 \\ 0 & 0 & A_{zz}{}^{\mathrm{II}} \end{pmatrix}\begin{pmatrix} S_x{}^{\mathrm{II}} \\ S_y{}^{\mathrm{II}} \\ S_z{}^{\mathrm{II}} \end{pmatrix}. \qquad (44) \end{aligned}$$

We shall substitute the values of $\langle S\rangle$ into this equation which are consistent with the values of $\langle\mu\rangle$ used for the dipole sum calculation, remembering that both orbit and spin contribute in some way to the dipole sum while in our approximation only the spin contributes to the hyperfine interaction. The $\pm$ signs in front of the off-diagonal yz terms in the first tensor reflect the fact that the two type I interactions are with two Ni^{++} ions above and below the xy plane whose off-diagonal interactions will cancel[22] at the fluorine site. Also, by symmetry considerations, all the other off-diagonal terms vanish as can be seen by inspecting Fig. 1(a). We can show from Eq. (44) that the hyperfine interactions expressed in terms of the moments and equivalent fields are

$$\begin{aligned} \mathbf{H}_{\mathrm{hf}}{}^{\mathrm{I}}=&-\frac{4\pi\langle\mu\rangle c}{\sqrt{2}g\beta\gamma_N}\begin{bmatrix} A_x{}^{\mathrm{I}}(\sin\theta_B-\cos\theta_B) \\ A_y{}^{\mathrm{I}}(\sin\theta_B+\cos\theta_B) \\ 0 \end{bmatrix},\\ \mathbf{H}_{\mathrm{hf}}{}^{\mathrm{II}}=&-\frac{2\pi\langle\mu\rangle c}{\sqrt{2}g\beta\gamma_N}\begin{bmatrix} A_x{}^{\mathrm{II}}(-\sin\theta_B+\cos\theta_B) \\ A_y{}^{\mathrm{II}}(\sin\theta_B+\cos\theta_B) \\ 0 \end{bmatrix}, \end{aligned} \qquad (45)$$

where now, having shown that the off-diagonal terms of the hyperfine interaction vanish, we have returned to the single subscript. By taking the components along a and b, introducing the numerical values of $\langle\mu\rangle$

$=-0.964g\beta$, $\gamma_N=2.52\times10^4$ sec^{-1} gauss^{-1}, and rearranging, the hyperfine interactions can be expressed as effective fields:

$$\begin{aligned}H_a=3.60\times10^2[&\sin\theta_B(2A_x^{\rm I}+2A_y^{\rm I}-A_x^{\rm II}-A_y^{\rm II})\\&+\cos\theta_B(-2A_x^{\rm I}+2A_y^{\rm I}-A_x^{\rm II}+A_y^{\rm II})],\\H_b=3.60\times10^2[&\sin\theta_B(-2A_x^{\rm I}+2A_y^{\rm I}-A_x^{\rm II}+A_y^{\rm II})\\&+\cos\theta_B(2A_x^{\rm I}+2A_y^{\rm I}+A_x^{\rm II}+A_y^{\rm II})].\end{aligned}\quad(46)$$

In these equations the A's are in units of 10^{-4} cm^{-1}. The experimental values of $H_i=10\,075$ gauss and $\varphi=101.3°$, in which φ is the angle between H_i and the [100] direction, can be reduced to $H_{ia}=9870$ gauss and $H_{ib}=-1974$ gauss. Since the dipole fields are given in Table VI, it is possible to calculate two parameters of the hyperfine interaction from the two relations in Eq. (46). By inspecting these relations it is obvious that the main contribution to H_a comes from the coefficient of $\sin\theta_B$. Furthermore, the most important term in this coefficient is $2A_s^{\rm I}-A_s^{\rm II}$, so that the experimental value of H_a is used to derive the values of $A_s^{\rm I}$ and $A_s^{\rm II}$ in Appendix A. The value of H_b, on the other hand, is very sensitive to small changes in $A_\sigma^{\rm I}$ and $A_\sigma^{\rm II}$. When these parameters are determined, as described in Appendix A, we obtain the perfectly reasonable values for the hyperfine interaction listed in Eq. (29) and compared with $KNiF_3$ in Table II. The values determined for $KNiF_3$ are unambiguous because of its cubic symmetry. It has been shown[3] that $KMnF_3$ agrees within experimental error with the values measured in MnF_2. Therefore we conclude that the values of the hyperfine interaction in NiF_2, which are determined from the spin ordering of Fig. 5, are the correct values. Consequently, we show that the limit of error of the spin ordering is $\pm1°$.

Another confirmation of the magnetic ordering is obtained when H_0 is rotated away from the [100] direction in the (001) plane. The resonance splits into two, one going to higher field and the other to lower, as illustrated in Fig. 6 for $\nu=44.110$ Mc/sec at $T=4.2°$K. Two different curves have been calculated with different assumptions. The solid line assumes that the spins do not move as H_0 is rotated—it assumes that $H_i=10\,070$ gauss and that the angle φ between H_i and the b axis remains constant during the experiment at 100.8° which is the angle calculated for $\theta=0$ in Eq. (38). The dashed line represents the H_0 expected for resonance if the spins move as the angle θ between H_0 and the b direction changes. By substituting the experimental values of H_0 and θ into Eq. (37) and Eq. (38), it was possible to calculate the changes in θ_A and θ_B. The new values of spin orientation were then substituted into Eq. (42) and Eq. (46) in order to evaluate the new value of H_i and the angle φ. In order to show the dependence of H_i upon θ, we have plotted in Fig. 7 the calculated values of the magnitude and angle of H_i as H_0 is rotated with respect to [100]. These values were computed for the experimental values of H_0 displayed in Fig. 6 under the conditions $T=4.2°$K and $\nu=44.110$ Mc/sec. Included in Fig. 7 are the dependences of θ_A and θ_B upon H_0 and its angle θ. It can be seen that θ_A and θ_B each varies by one half of a degree in this range. The concomitant variation of the angle φ is about twice as great. In Fig. 6 we see that the lack of agreement between the calculated curves and the experimental points is on the average equal to the differences between the two calculated curves. For $H_0\sim10°$ from the [100] direction, this difference reflects a little less than 1° difference in the angle φ. This is an independent confirmation that the internal field is as calculated from the data of Table V.

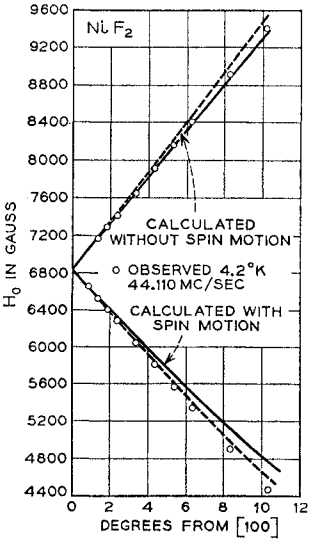

FIG. 6. Splitting of the F^{19} resonance at $T=20.3°$K as H_0 is rotated away from the [100] direction in the (001) plane.

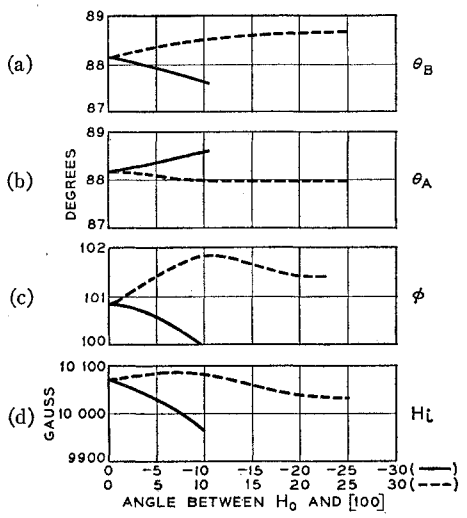

FIG. 7. (a) and (b) The calculated variation of the spin angles θ_A and θ_B defined in Fig. 5 as H_0 is rotated in the (001) plotted as a function of angle θ between H_0 and [100] under the same experimental conditions as Fig. 6. In all four parts of this figure, the solid curve corresponds to the smaller value of H_0 and the dashed curve to the larger. (c) Calculated variation in the angle φ between H_i and the [100] direction as a function of the angle θ between H_i and the [100]. (d) Calculation variation in the magnitude of H_i with θ.

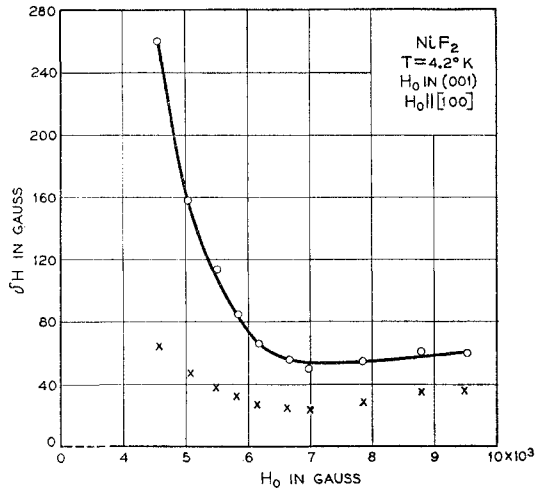

FIG. 8. The observed intervals between derivative extrema, δH, at $T=4.2°$K with $H_0\|[100]$ are plotted as circles. The angle between H_0 and the resultant field at the nucleus varies, as shown in the text, as H_0 is changed so that the corrected widths are plotted as crosses.

LINEWIDTHS IN ANTIFERROMAGNETIC STATE

In the paramagnetic region the observed linewidths have been explained by the exchange narrowing mechanism previously observed to be responsible for linewidths in other paramagnetic iron group fluorides. In the antiferromagnetic region the observed linewidths shown as circles are functions of H_0 as shown in Fig. 8 and Fig. 9. Figure 8 shows the separation between extrema of the derivative of the single absorption line observed for $H_0\|[100]$ at 4.2°K at different values of H_0. The same measurements for the two separate lines observed at the same temperature, but with H_0 just far enough away from [100] in the (001) plane so that the two lines are well resolved, are shown in Fig. 9. Both sets of measurements were made with magnetic field modulation. It is evident from these plots that, as H_0 is decreased from ~5000 gauss, the individual resonances broaden rapidly. By extrapolating to zero field the resonances would be more than a thousand gauss wide.

This measured increase of the linewidths, in gauss, as H_0 is decreased is caused by the resultant field at the nuclei being far from parallel to H_0. In fact, by differentiating Eq. (36) we can show that

$$\frac{\partial H_r}{\partial H_0}=\frac{H_0-1974}{\omega/\gamma_N}, \tag{47}$$

in which H_r is the resultant field at the nuclei. If we correct the data for these geometrical considerations, we obtain the true values of δH shown as crosses and hollow squares in Fig. 8 and Fig. 9. The crosses and squares in the latter distinguish between the resonances observed at higher and lower fields, respectively, for the same orientation. As zero field is approached, the resonance decreases in strength because magnetic field modulation was used. The modulation field is parallel to H_0 and is attenuated in the same way as H_0. The resonance was not seen at zero field with magnetic field modulation consisting of a clipped sine wave based on zero. This led to the conclusion that either most of the ferromagnetic moments were aligned by the modulation field which, during the half cycle it was on, averaged ten gauss; or second, it was possible that the broadening noticed in the corrected data of Fig. 8 indicates a trend and the resonance is really very broad at low fields.

From Fig. 9 the average width of the individual resonances is seen to be ~25 gauss. Nakamura[34] and Suhl[35] have explained nuclear resonance linewidths in ordered magnetic substances by indirect exchange interactions. Nakamura[34] has shown that the width of the

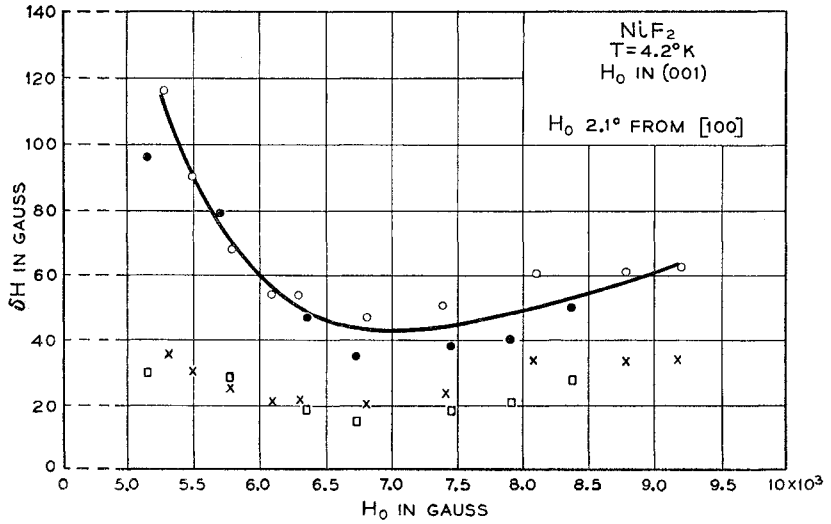

FIG. 9. Dependence of δH upon H_0 with H_0 2.1° from the [100] direction in the (001) plane. Open circles refer to measurements of the lower field line, solid circles to the line which is displaced to higher fields. The corresponding corrected values are shown as crosses and squares, respectively.

[34] T. Nakamura, Prog. Theoret. Phys. (Kyoto) **20**, 542 (1958).
[35] H. Suhl, Phys. Rev. **109**, 606 (1958).

F^{19} resonance observed[19] in MnF_2 can be explained by an indirect coupling of nuclear spins via the excited spin-wave states. This is analogous to the Ruderman-Kittel,[36] Bloembergen-Rowland[37] indirect exchange mechanism. The main difference in the results obtained is that in antiferromagnetic materials the broadening only occurs as a result of interactions between identical nuclei. For MnF_2, Nakamura has calculated the second moment, ΔH_2^2, of the F^{19} resonance to be

$$\Delta H_2^2=\left(\frac{\gamma_N}{2\pi}\right)^{-2}\times\tfrac{2}{3}I(I+1)\left(\frac{A^2}{2\hbar\omega_e}\right)^2 f', \qquad (48)$$

in which A is the hyperfine interaction per bond, ω_e is the exchange frequency, and I and γ_N refer to fluorine. The factor f' for the case of small anisotropy is given by

$$f'\cong 40/\pi\Delta, \qquad (49)$$

in which $\Delta=(2H_A/H_E)^{\frac{1}{2}}$, where H_A is the anisotropy field and H_E is the exchange field. We have reduced f' by a factor of two because only one of the two spin-wave branches in NiF_2 is contributing. Notice that if the anisotropy is small then f' is large and the line is broadened. We can evaluate Δ by using Moriya's[8] expression for the antiferromagnetic resonance frequency as follows:

$$\omega_2=2A_2\omega_e=0.06\gamma H_E=\gamma(2H_AH_E)^{\frac{1}{2}}. \qquad (50)$$

Since from the torque[6,8] measurements $A_2=0.03$, then

$$\Delta=0.06. \qquad (51)$$

Calculating the exchange energy from the Néel temperature in the same way as was done[34] for MnF_2, and substituting in Eq. (48), with the relation for Gaussian lines that

$$\Delta H_2^2=\tfrac{1}{4}\delta H^2, \qquad (52)$$

we calculate that

$$\delta H=33 \text{ gauss}. \qquad (53)$$

This is a good fit to the experimental value of $\sim$25 gauss, considering the simplifications of both theory and experiment. The indirect coupling predicts larger widths in NiF_2 than in MnF_2 because in the former the anisotropy is smaller and the hyperfine coupling to the fluorides is larger. The anisotropy is small because the 90° symmetry of the sites in the (001) plane would give zero anisotropy for a 180° spin alignment in that plane, while the ordering observed differs from 180° by only $\sim$3°.

TRANSITION REGION

In this section, the nuclear resonance results obtained as the temperature is lowered from 298°K through $T_N=73.2°$ will be discussed. The experimental values of the fractional resonance shifts $\alpha\equiv\Delta H/H_0$ at 298°K, 90.3°K, and 77.3°K are listed in Table I. In the last column of the table are listed the values of α divided by the spin-dependent portion of the susceptibility as defined in Eq. (8). This number should be a constant since it is proportional to the spin-independent factors of the hyperfine interaction and dipole sum. It can be seen from Table I that it is constant, to within experimental accuracy, for $H_0\|[001]$. However, it is not constant for $H_0\|[110]$ as can be seen from those data. In fact, as the temperature is lowered close to T_N, some of the nuclear resonance shifts begin to vary very rapidly with temperature as shown in Fig. 10. In this figure the magnetic field required for resonance at the constant frequency of 44.874 Mc/sec is plotted vs temperature.

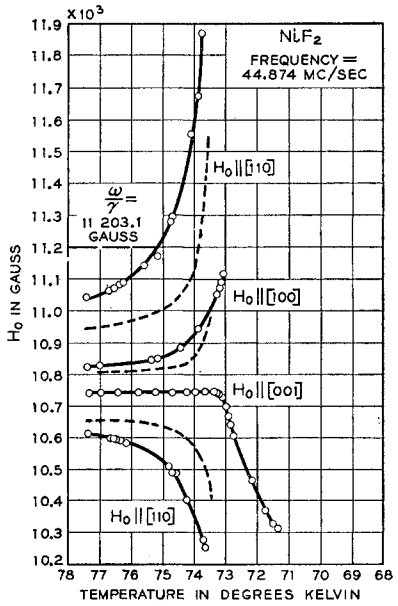

FIG. 10. Measurements of H_0 vs temperature for three different orientations. The dashed line represents the calculated values of the shift as described in text.

Let us first consider the results obtained with $H_0\|[001]$ since these are the least anomalous. In the region from 77.3°K to 73.2°K, the single resonance stays constant at $H_0=10\,742$ gauss. The resonance is 17.9 gauss wide in this region and the width was constant between 77.3°K and 73.2°K. The measurements shown in Fig. 10 taken with $H_0\|[001]$ show less than one gauss variation of ΔH with temperature. Actually a change in ΔH of about nine gauss is expected over this temperature range because of the change of susceptibility with temperature. However, the displacement is very sensitive to the error made in aligning the crystal. When small errors in alignment were made, the resonance was observed to shift to higher fields as $T\rightarrow T_N$, indicating some admixture of the perpendicular components which does shift to higher fields. Disregarding these small orientation effects, the results with $H_0\|[001]$ were very similar to our previously[1] reported measurements in MnF_2 where α followed the susceptibility right

[36] M. A. Ruderman and C. Kittel, Phys. Rev. **96**, 99 (1954).
[37] N. Bloembergen and T. J. Rowland, Phys. Rev. **97**, 1679 (1955).

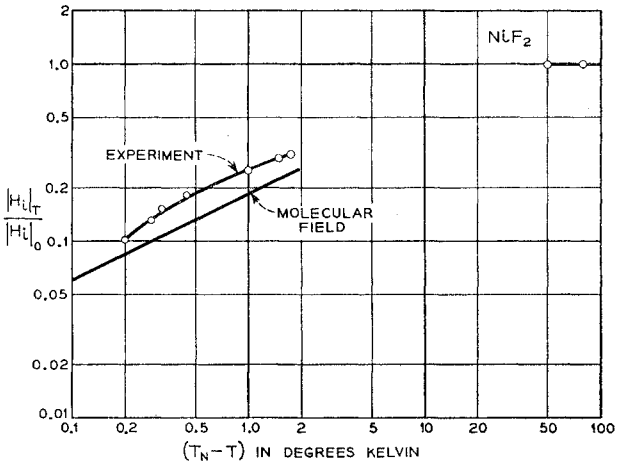

FIG. 11. Calculated values of H_i vs temperature as a result of measurements made near T_N and at 20.3°K and 4.2°K. The fit was made to a Brillouin function.

down to T_N and in which the susceptibility was a well-behaved gently varying function of temperature. At 73.2°, corresponding to T_N, the resonance field begins to change rapidly with temperature. The reason for this is that the internal field H_i, following the sublattice magnetization, is growing rapidly as the temperature is lowered in this region. The first interesting point, as shown in Fig. 10, is that the resonance field is continuous across T_N. The resonance did not disappear as the temperature was cycled through T_N. This is to be expected as $\chi_{\parallel}$ should be continuous across T_N. Just below T_N the resonance became a little narrower and more intense, but several degrees below T_N it broadened and disappeared. Since the internal field H_i is known from our measurements at $T \ll T_N$ to lie in the (001) plane, it can be measured in this temperature region in the following way. With $H_i \perp H_0$, Eq. (36) reduces to

$$H_i^2+H_0^2=(\omega/\gamma_N)^2=(11\,203.1)^2, \tag{54}$$

at the conditions of the experiment. The values of H_i calculated are plotted in Fig. 11 along with the values measured at 20.3°K and 4.2°K. An attempt has been made to fit these points with the Brillouin[28] function which is plotted as a solid line in Fig. 11. It can be seen that the agreement is not bad but that a more detailed comparison would be afforded by measurements of H_i at intermediate temperatures. Unfortunately, below 71.5°K the lines broaden and disappear. First we shall consider the possibility that they disappear because of temperature inhomogeneities across the sample broadening the resonance. Differentiating Eq. (54), we have

$$\frac{\partial H_0}{\partial T}=-\frac{H_0}{H_i}\frac{\partial H_i}{\partial T}. \tag{55}$$

Substituting measured values of H_i, H_0 and setting $\Delta H_i/\Delta T \sim \partial H_i/\partial T$ gives a maximum value of $\partial H_0/\partial T \cong 500$ gauss/degree at $T \sim 72.8$°K. At $T \sim 71.5$°K, where the resonance disappears, the value is $\partial H_0/\partial T \cong 160$ gauss/degree. These effects will not explain the decrease in fluorine resonance intensity unless one assumes that the temperature gradients across the sample increase enough as the temperature is lowered to overcompensate the decreasing value of $\partial H_0/\partial T$ with decreasing temperature. Since there is no reason to expect this, we must look for another reason.

The line disappears at 71.5° with $H_0 \| [001]$ in a way that is consistent with the disappearance of the resonance in the antiferromagnetic region for $H_0 \| [100]$. As is shown in Fig. 8, as the magnetic field parallel to [100] is reduced and magnetic field modulation is used, the resonance begins to broaden until it becomes too broad to observe. With $H_0 \| [001]$ it is perpendicular to H_i which is in the (001) plane. As H_i increases, the effect of the modulation field upon the resultant decreases and the resonance becomes apparently broader and steadily weaker as described in Eq. (47).

It can be seen from the last column of Table I that although α/χ is well behaved for $H_0 \| [001]$, it is not well behaved for H_0 in the (001) plane. These results for the temperature region just above T_N are shown in Fig. 10. The rapidly varying shifts of the fluorine resonance could be explained by a rapidly varying susceptibility in this region, which would be similar to the variations in a ferromagnetic substance just above its Curie temperature. Stimulated by these results, we gave a single crystal of NiF_2 to Cooke and Lazenby to measure the susceptibility in this temperature region. Their measurements[20] of $\chi_{\perp}$ show a rapid increase as the temperature is lowered towards T_N. Measuring the molar susceptibility along the direction of maximum susceptibility in the (001) plane, they find that $\chi_{\perp}=6.17\times10^{-3}$ cm³/mole at 90.0°K and 6.37×10^{-3} cm³/mole at 77.05°K, after which it rises rapidly to 8.23×10^{-3} at 73.4°K. The susceptibility of NiF_2 has been calculated by Moriya[8] from the spin Hamiltonian. Moriya has extended his calculations so as to include enough separate contributions to the susceptibility to explain these results. With his encouragement we present the salient features of the derivation.

In place of his Eq. (3.1) for $\chi_{\perp}$ we can write the temperature-dependent part of $\chi_{\perp}$ for the two different sublattices labeled A and B in Fig. 1. Along the [110] direction these are

$$\chi_{[110]}{}^A-\chi_{\infty}{}^A=\frac{1}{F}\frac{2g_1^2\beta^2\delta_1}{D-E}\times\left\{1-\frac{2\delta_2}{D+E}\left(\frac{g_2}{g_1}J-J'\right)\right\}\equiv\chi_x{}^0, \tag{56}$$

$$\chi_{[110]}{}^B-\chi_{\infty}{}^B=\frac{1}{F}\frac{2g_2^2\beta^2\delta_2}{D+E}\times\left\{1-\frac{2\delta_1}{D-E}\left(\frac{g_1}{g_2}J-J'\right)\right\}\equiv\chi_y{}^0, \tag{57}$$

in which we have defined the quantities χ_x^0 and χ_y^0 to be the temperature-dependent parts of the susceptibilities along the x and y directions of Fig. 1(b).

The total susceptibility in the (001) plane is

$$\chi_\perp-\chi_{\perp\infty}=\frac{\beta^2}{F}\Big\{g_1^2\frac{\delta_1}{D-E}+g_2^2\frac{\delta_2}{D+E}+[(g_1-g_2)^2(J+J')-(g_1^2+g_2^2)(J-J')]\frac{\delta_1\delta_2}{D^2-E^2}\Big\}, \quad (58)$$

in which

$$F=1+2J'\left(\frac{\delta_1}{D-E}+\frac{\delta_2}{D+E}\right)-4(J^2-J'^2)\frac{\delta_1\delta_2}{D^2-E^2},$$

and

$$J=8J_1,$$
$$J'=2J_2+4J_3,$$

where J_1 is the exchange coupling between a nickel ion on one sublattice and its eight near neighbor nickel ions from the other sublattice. This is the predominant antiferromagnetic coupling while the couplings with other nickel ions on the same sublattice are described by J_2 and J_3. In this expression,

$$\frac{\delta_1}{D-E}=\frac{1}{3kT}\left[1+\frac{D+3E}{6kT}-\frac{D^2+3E^2}{2(3kT)^2}+\cdots\right], \quad (59)$$

and

$$\frac{\delta_2}{D+E}=\frac{1}{3kT}\left[1+\frac{D-3E}{6kT}-\frac{D^2+3E^2}{2(3kT)^2}+\cdots\right]. \quad (60)$$

Now upon defining T_N as the temperature at which $F=0$, we find that

$$\chi_x^0=\frac{2g_1^2\beta^2}{3k}\left(1+\frac{D}{3kT}+\cdots\right)\times\frac{T-T_1}{(T-T_N)(T+\theta+\eta/T+\cdots)}, \quad (61)$$

$$\chi_y^0=\frac{2g_2^2\beta^2}{3k}\left(1+\frac{D}{3kT}+\cdots\right)\times\frac{T-T_2}{(T-T_N)(T+\theta+\eta/T+\cdots)}, \quad (62)$$

in which

$$T_1=T_N+\frac{2}{3k}\left[-\left(\frac{g_1-g_2}{g_1}J+\frac{3E}{4}\right)+\frac{3DE}{8(J-J')}-\frac{9E^2}{32J}\right], \quad (63)$$

and

$$T_2=T_N+\frac{2}{3k}\left[+\left(\frac{g_1-g_2}{g_2}J+\frac{3E}{4}\right)-\frac{3DE}{8(J-J')}-\frac{9E^2}{32J}\right], \quad (64)$$

and

$$\theta=T_N+4J'/3k, \quad (65)$$

$$\eta=(2/3k)^2(D/2)(J+J')+\cdots. \quad (66)$$

In addition to these relations for the individual sublattices, we also have for the perpendicular susceptibility

$$\chi_\perp-\chi_{\perp\infty}=\frac{(g_1^2+g_2^2)\beta^2}{3k}\left(1+\frac{D}{3kT}+\cdots\right)\times\frac{T-T_0}{(T-T_N)(T+\theta+\eta/T+\cdots)}, \quad (67)$$

in which

$$T_0=T_N-\frac{2}{3k}\left[\frac{9E^2}{32J}+\frac{3E^2}{2|\lambda|}+\frac{2E^2J}{\lambda^2}+\cdots\right]. \quad (68)$$

Hence, we see that there are four temperatures necessary to describe the susceptibility in this region. Furthermore, g_1 and g_2 are the g factors defined as $g_1=g_{[110]^A}=g_{[1\bar{1}0]^B}=g_x$ and $g_2=g_{[110]^B}=g_{[1\bar{1}0]^A}=g_y$. There is an ambiguity left because from the electron spin resonance results[21] we do not know the sign of E in the spin Hamiltonian; we only know its magnitude. This ambiguity is removed by the present measurements by which it has been determined, as shown below, that the sign of E is negative using the coordinate system of Fig. 1(b).

With these expressions it is possible to calculate that

$$T_1=T_N+2.52°=75.74°\text{K}, \quad (69)$$

$$T_2=T_N-2.56°=70.66°\text{K}, \quad (70)$$

$$T_0=T_N-0.07°=73.15°\text{K}, \quad (71)$$

where we have used the value $T_N=73.22°$K and in which it has been assumed that $J'=35$ cm^{-1}. The value of $(T+\theta+\eta/T+\cdots)$ is slowly converging in this temperature region, and when evaluated from Eqs. (65) and (66) gives $73.2+67+6.7+\cdots=147°$K. By fitting Cooke and Lazenby's measured[20] values of $\chi_\perp$, a better value for $T_N+\Theta+\eta/T+\cdots$ is 158°K. Our plan is to see how well the observed fluorine resonance positions shown in Fig. 10 can be fit by these expressions for the susceptibilities. Substituting numerical values in Eq. (61) and Eq. (62), we have

$$\chi_x^0=1.395\frac{T-75.74}{(T-73.22)(T+158)}, \quad (72)$$

$$\chi_y^0=1.405\frac{T-70.66}{(T-73.22)(T+158)}. \quad (73)$$

For $75.74>T>73.22$, χ_x^0 is actually negative. Furthermore, these two equations are derived on the assumption that $E<0$. If we assume that $E>0$, then χ_x^0 and χ_y^0 would be interchanged because changing the sign of E interchanges the values of g_1 and g_2 as shown in Eqs. (19) and (20). In order to distinguish between these alternatives and to ascertain the agreement between theory and experiment, we shall try to fit the experimental results for $H_0\|[110]$. Two lines are observed, as discussed in the previous section, corresponding to the two different fluorine sites. The more displaced resonance corresponds to a hyperfine interaction of $2A_y^{\mathrm{I}}\langle S_y^{\mathrm{I}}\rangle + A_x^{\mathrm{II}}\langle S_x^{\mathrm{II}}\rangle$, the less displaced to an interaction $2A_x^{\mathrm{I}}\langle S_x^{\mathrm{I}}\rangle + A_y^{\mathrm{II}}\langle S_y^{\mathrm{II}}\rangle$. Using the relations of Eqs. (4) and (5), we can write the fractional shifts of all three resonance lines in the (001) planes in terms of the susceptibilities of the two sublattices. Doing this so as to include both hyperfine interactions and the dipole sums, we have

$$\alpha_{[110]}=(0.1152A_y^{\mathrm{I}}+0.076)\chi_y^0 + (0.0567A_x^{\mathrm{II}}+0.366)\chi_x^0, \quad (74)$$

$$\alpha_{[1\bar{1}0]}=(0.1152A_x^{\mathrm{I}}-0.367)\chi_x^0 + (0.0576A_y^{\mathrm{II}}-0.159)\chi_y^0, \quad (75)$$

$$\alpha_{[100]}=(0.1152A_z^{\mathrm{I}}+0.0576A_z^{\mathrm{II}}+0.0837)\chi_{\mathrm{II}}^0, \quad (76)$$

in which we have set $\chi_z^0=\chi_{\mathrm{II}}^0$. It can be seen from Fig. 10 that the most rapid variation of α with temperature in the transition region occurs for the lines with H_0 parallel to [110] and [1$\bar{1}$0]. The numerical values of χ_y^0 and χ_x^0 are determined by Eqs. (72) and (73), while the dipole sums and hyperfine interactions are determined by Eq. (9) and Eq. (29), respectively. In Fig. 10 we have presented the measured shifts and the values calculated for H_0 in the (001) plane from Eq. (74) and Eq. (75). It can be seen that, as a first approximation, the two-sublattice model of the susceptibility explains the nuclear resonance shifts observed in this temperature region. Furthermore, although the experimental results show that α changes a bit more gradually than the calculated, *still it must be remembered that there are no adjustable parameters in the calculated values*. All the terms have either been measured independently or else have been deduced from measured quantities.

This rapid variation of susceptibility was first observed in powdered NiF_2 in collaboration with Jaccarino several years ago by noticing the rapid increase in the width of the F^{19} resonance in the powder. There is reason to believe that this rapid change of susceptibility is a general property of weak ferromagnets because anhydrous CrF_3 powder also has shown[38] the same broadening while neutron diffraction measurements[39] coupled with susceptibility studies[40] show CrF_3 to be a weak ferromagnet.

Between the preliminary announcement[41] of our determination of the magnetic ordering in NiF_2 and this final report, an independent neutron diffraction reinvestigation of the magnetic ordering has been reported by Alikhanov,[42] who has reached the same conclusion about the direction of spin alignment as we have.

ACKNOWLEDGMENTS

As indicated at various points in the text, this investigation has profited from Dr. T. Moriya's parallel study. In addition we should like to acknowledge with gratitude the helpful way by which Dr. Moriya has clarified our understanding in personal conversations. It is a pleasure to thank B. J. Wyluda for his help in all parts of the experimental investigation. Without the large single crystals ingeniously grown by H. Guggenheim this work could not have been done. We would like to thank H. R. Moore who, with H. G. Hopper's assistance, designed and constructed the variable-frequency spectrometer; Professor J. W. Stout for indicating the proper way to grow single crystals of NiF_2, and Mrs. M. H. Read who kindly oriented the crystals used in this study.

Part of this research was done while the author was visiting the Fysisk-Kemisk Institut of the University of Copenhagen under a grant from the Rask-Oersted Foundation. It is a pleasure to acknowledge this support and to thank Professor C. J. Ballhausen for his hospitality during this period.

APPENDIX A

In this Appendix we calculate the components of the hyperfine interaction tensor, using three measurements from the paramagnetic state and two from the antiferromagnetic state. For the antiferromagnetic state we *assume* the spin ordering calculated by Moriya and shown in Fig. 5. The values of the hyperfine interactions obtained are shown to agree with those measured in $KNiF_3$ where their interpretation was unambiguous because of the cubic symmetry. Finally, in this section, we investigate the effect of departures from Moriya's model upon the values of the hyperfine interaction and conclude that his model of spin ordering is correct with an error limit of $\pm$ one degree.

Seven independent measurements of the magnetic field at the fluorine nuclei are reported in this paper. In the paramagnetic state three independent measurements are made; in the transition region two different combinations; in the antiferromagnetic region two different combinations of the A's are measured, i.e., the direction and magnitude of the internal field at the fluorine sites in the domains. As discussed in the section on the paramagnetic state, it is a good first approximation to describe the fluorine hyperfine interaction in terms of

[38] K. Knox, R. G. Shulman, and T. R. Waite (to be published).
[39] E. O. Wollan, H. R. Child, W. C. Koehler, and M. K. Wilkinson, Phys. Rev. **112**, 1132 (1958).
[40] W. N. Hansen and M. Griffel, J. Chem. Phys. **30**, 913 (1959).
[41] R. G. Shulman, Proceedings of Radio-Frequency Spectroscopy Conference, Oxford, September, 1959 (unpublished).
[42] R. A. Alikhanov, J. Exptl. Theoret. Phys. (U.S.S.R.) **37**, 1145 (1959) [translation: Soviet Phys.-JETP **10**, 814 (1960)].

four coupling constants, A_s^{I}, A_s^{II}, A_σ^{I}, and A_σ^{II}. In order to determine these A's it is necessary to know $\langle S\rangle$. As shown in the text, $\langle S\rangle$ in the paramagnetic state is known quite accurately, while in this state three independent measurements of the A's can be made. By adding another variable, i.e., the angle θ which the unpaired p_σ electrons really make with the z axis, and by allowing this to differ from the angle between the z axis and the internuclear radius, we introduce one more degree of freedom. In our opinion the spin alignment is known more accurately in the antiferromagnetic state than it is in the transition region. Therefore, our procedure will be to use the two parameters measured in the antiferromagnetic state in conjunction with the three from the paramagnetic state to determine the A's. When this is done, we find that the five parameters so determined are (in units of 10^{-4} cm^{-1})

$$\begin{aligned} &A_s^{I}=36.4\pm1.8, \quad A_\sigma^{I}=9.1\pm0.9,\\ &A_s^{II}=42.1\pm2.1, \quad A_\sigma^{II}=9.9\pm0.9, \qquad \text{(A-1)}\\ &\theta_{y,\sigma}=54.0^\circ. \end{aligned}$$

The angle of 54.0° differs slightly but significantly from the angle of 50.1°. A reasonable upper limit on the unpaired spin introduced into the fluorine π bonds, which we have assumed to be zero, would be the σ contribution multiplied by the sin4° or $\sim0.7\times10^{-4}$ cm^{-1}. In order to obtain the positive values of A_σ^{I} and A_σ^{II} in Eq. (A-1), it was necessary to use the values of Eq. (25). The alternative values of Eq. (26) lead to unrealistic negative values of these quantities.

To obtain values of the individual components of the hyperfine interaction tensor, we substitute Eq. (A-1) into Eq. (28) with the results, in units of 10^{-4} cm^{-1},

$$\begin{aligned} &A_x^{I}=27.3\pm2.0, \quad A_x^{II}=61.9\pm2.5,\\ &A_y^{I}=36.7\pm1.8, \quad A_y^{II}=32.2\pm2.3, \qquad \text{(A-2)}\\ &A_z^{I}=45.2\pm2.0, \quad A_z^{II}=32.2\pm2.3. \end{aligned}$$

These values are our best fit of the data and are used throughout this paper unless otherwise specified. There are three important sources of error in these determinations, whose contributions to the errors in A we estimate as follows. First, there is the neglect of π bond formation which might contribute as much as $\pm0.7\times10^{-4}$ cm^{-1} to the p_σ interactions. Second, there are uncertainties in the spin alignments in both paramagnetic and antiferromagnetic states. In the paramagnetic state the possible errors in the susceptibility might be as large as $\pm3\%$. Since the dipole sum is only about one quarter of the observed anisotropy, the uncertainty in the susceptibility is no more important to the p_σ contribution than to the isotropic part. To all parts it contributes a 3% uncertainty. Below T_N we consider the effect of a spin deviation of one half of a degree from the values in Table VI. This would make a negligible contribution to the uncertainties of A_s^{I} and A_s^{II}. The effects of these variations upon A_σ^{I} and A_σ^{II} is seen most directly by considering the expressions for the a and b components of H_i in the antiferromagnetic state given in Eq. (46).

Considering H_b, it can be seen that if θ_B changes by $\pm$ one half of a degree from the value of 88.20 at $H_0=6000$ gauss, then $\cos\theta_B=0.0314\pm0.009$. Now from Eq. (25) the coefficient of $\cos\theta_B$ is 222.1×10^{-4} cm^{-1}, which allows a possible error of $\pm2\times10^{-4}$ cm^{-1} in this term. This allows an error of $\pm0.4\times10^{-4}$ cm^{-1} to appear in the individual values of A_σ^{I} and A_σ^{II}. The third source of errors are experimental inaccuracies. In the paramagnetic state these are estimated to $\pm2\%$ in the value of the shifts. In the antiferromagnetic state they are negligible. These last considerations of spin alignment and experimental errors, considered together, introduce a possible error of $\pm0.6\times10^{-4}$ cm^{-1} into the values of A_σ^{I} and A_σ^{II}.

We have neglected possible changes in the values of A with temperature which would be associated with thermal expansion. If the thermal expansion is the same as in MnF_2, we can estimate that the errors introduced are negligible.

From these considerations we see that although the values of A_σ^{I} and A_σ^{II} would be negligibly affected by an error of $\pm$ one half of a degree in the spin order, still an error of $\pm$ one degree would change the values by an amount equal to the possible errors. Taking the reduction of the NiF_2 p_σ values by π bonding into account, we see from Table II that within experimental errors the bonding is the same in NiF_2 and $KNiF_3$. Since the cumulative errors correspond to an uncertainty of $\pm$ one degree in the spin order, we can take that to be the accuracy with which we have confirmed the spin order.